ORIGINAL ARTICLE

In situ biosynthesis of palladium nanoparticles on banana leaves extract-coated graphitic carbon nitride: An efficient and reusable heterogeneous catalyst for organic transformations and antimicrobial agent

Harini G. Sampatkumar[1] · Arnet Maria Antony[1] · Mansi Trivedi[2] · Manmohan Sharma[2] · Manjunath Ghate[2] · Mahiuddin Baidya[3] · Ramesh B. Dateer[1] · Siddappa A. Patil[1]

Abstract

In the present work, palladium nanoparticles embedded on banana leaves extract-modified graphitic carbon nitride [PdNPs@g-C_3N_4-BLE] was biogenically synthesized in a facile 3-step reaction in a clean and sustainable manner. In situ reduction of Pd(II) to Pd(0) was accomplished by the action of active phytochemicals present in the banana leaves extract as capping, reducing, and stabilizing agents. Therefore, the aforementioned synthesis of catalyst does not need toxic reagents, harsh conditions, and additional reductants. The structure and composition of the PdNPs@g-C_3N_4-BLE nanocatalyst were examined in detail through several spectroscopic and microscopic techniques. The PdNPs@g-C_3N_4-BLE nanocatalyst exhibited good catalytic activity in Suzuki–Miyaura cross-coupling and aryl halide cyanation reactions by giving high turnover numbers (TONs) and turnover frequencies (TOFs). The outstanding advantages of using the PdNPs@g-C_3N_4-BLE nanocatalyst are mild reaction conditions, short reaction time, heterogeneous nature, excellent yields, easy work-up procedure, and recyclability without any significant loss of catalytic activity. Additionally, the PdNPs@g-C_3N_4-BLE nanocatalyst showed remarkable antibacterial activity against gram-negative bacteria *Escherichia coli* and gram-positive bacteria *Bacillus subtilis*.

Keywords Graphitic carbon nitride · Banana leaves · Palladium nanoparticles · Suzuki–Miyaura cross-coupling · Cyanation reaction · Antimicrobial activity

1 Introduction

The theory of evolution, although enthralled by the topic of nanoscience, is the preponderance of the contemporary discussions, definitions, and attention centered on nanotechnology. Nanotechnology is concerned with the exploration of new nano systems in the physical, chemical, and the biological world [1]. The fascination with the nanoscale materials arose from the acquisition of new traits at nano scale, and how the changes in size and shape attribute to change in properties [2]. By replacing traditional bulk materials with equivalent nanoparticles (NPs), we can provide environmentally acceptable and cost-effective approaches for transforming basic materials into valuable chemicals [3], and thereby enhance and use them as active and stable heterogeneous catalysts [4, 5].

In majority of the organic reactions, noble metals have been commonly utilized as catalysts. Amidst the noble metals, palladium has unique characteristics such as excellent activity, selectivity, and stability under diverse reaction circumstances [6, 7]. As a result, it has a high value in catalytic systems [8]. Green synthesis of metal NPs has received a lot of interest in recent years due to its inexpensive and sustainable approach [9] as it covers a broad area in today's research. To reduce metal to metal NPs, the use of

✉ Siddappa A. Patil
p.siddappa@jainuniversity.ac.in; patilsiddappa@gmail.com

1 Centre for Nano and Material Sciences, Jain University, Jain Global Campus, Kanakapura, Ramanagara, Bangalore 562112, India

2 Institute of Pharmacy, Nirma University, Sarkhej-Gandhinagar Highway, Ahmedabad 382481, Gujarat, India

3 Department of Chemistry, Indian Institute of Technology Madras, Chennai 600036, India

phytochemicals as reducing agents [10] is a straightforward way towards green synthesis of NPs. These phytochemicals are found abundantly in plant sources such as leaves, stems, bark, pods, flowers, and fruits [11, 12]. Typically, after the crop harvest, a large quantity of plant-based waste materials is produced. One such plant waste is of banana, an herbaceous plant of the species *Musa acuminate* [13], which is obtained after fruitage [14]. The biocompatibility and nontoxicity of banana leaves are marked by their use in cooking and serving food, as they enhance the flavor and aroma of the food [15].

On the other hand, catalytic activity is affected by surface area. The larger the surface area, the higher the rate. Such a large surface area available on NPs, however, is constricted by the process of agglomeration [16]. As a result, researchers have used several solid supports, such as clays, carbon-based materials, silica, and other materials to disperse the metal NPs and thereby increase their catalytic efficiency [17, 18]. Due to the flourishing studies of graphene-based nanomaterials, two-dimensional nanosheet-based composite materials have garnered substantial attention and have become one of the hot study fields of nano chemistry. Carbon nitride (C_3N_4) is made up of carbon and nitrogen atoms in an alternating manner. It is divided into three allotropes which are graphitic, crystalline, and molecular. Among them, the graphitic phase is analogous to graphene, and being very stable under ambient conditions is of particular relevance due to its unusual chemical and electrical properties. Graphitic carbon nitride (g-C_3N_4) is composed of stacked tri-s-triazine subunits linked via planar tertiary amino groups within a layer. The presence of nitrogen atoms in g-C_3N_4 attributes to its unique qualities such as semiconductor properties and complexing ability, excellent chemical (pH 1–14), and thermal stability (up to 600 °C), making it a better material than graphene in various ways, possibly the best among organic materials [19]. As a result, g-C_3N_4 has been employed in heterogeneous catalysis [20, 21], used as a suitable supporting material in electrochemical sensors, hydrocarbon oxidation, and optoelectronic conversion, among other things [22, 23].

In organic transformations, Suzuki–Miyaura cross-coupling reaction has obtained a lot of interest since its first appearance in the scientific community in the year 1979, owing to its adaptability in the creation of carbon–carbon (C–C) bonds [24]. Precisely, for biaryl construction, this cross-coupling has established itself as the "gold standard" [25]. As a result, it is the most commonly used reaction in drug discovery, synthesis of natural products and agrochemicals, more specifically for carrying out $C(sp^2)$–$C(sp^2)$ cross-couplings. Furthermore, as compared to other cross-coupling reactions like Kumada, Heck, Stille, Sonogoshira, and Fukuyama, Suzuki–Miyaura cross-coupling reaction has some advantages such as high tolerance towards diverse functional groups, ease of availability, and high stability of

employed substrates [26]. Also, compared to other organometallic reagents, organoboranes are environment friendly and can be easily removed from the reaction medium, especially in large-scale synthesis [27]. Hence, one of the most efficient techniques extensively used for the formation of C–C bonds in industrial and academic research is the palladium catalyzed Suzuki–Miyaura cross-coupling reaction [28]. However, homogeneous catalytic systems have significant limitations such as severe reaction conditions, byproduct formation, difficulty in separation of final product, and recovery and reusability of the catalyst. These issues can be addressed by using heterogeneous catalysts prepared by immobilizing the catalyst onto an inert support. These catalytic systems have the advantages of enriched catalytic activity, low metal leaching and high reusability under ambient conditions [29–33].

The nitrile group (-C≡N) present in aryl nitriles are extensively used as building blocks in a wide range of synthetic organic chemistry applications such as agrochemicals, herbicides, pharmaceuticals, and natural materials, owing to their versatility [34]. The nitrile group can be easily transformed into other functionalities such as amides, carboxylic acids, aldehydes, ketones, or amines, making them a fundamental functional group in synthetic organic chemistry. Metal catalyzed cyanation of aryl halides is the frequently used process for synthesizing aryl nitriles. Previously, stoichiometric concentrations of highly poisonous cyanating reagents such as zinc cyanide, potassium cyanide, copper cyanide, sodium cyanide, and trimethylsilyl cyanide (TMSCN) [35–37], or expensive and hazardous cyanating reagents such as benzyl thiocyanates, phenyl cyanates and acetone cyanohydrins [38, 39] were utilized to synthesize aryl nitriles. To overcome these problems, Beller et al. were the first to employ potassium hexacyanoferrate(II) trihydrate [$K_4Fe(CN)_6$].$3H_2O$ as a cyanide source in cyanation reactions due to its nonpoisonous, low cost, and environmental friendly nature [40]. Additionally, several Pd NPs supported on inert materials were developed as heterogeneous catalysts and employed in the cyanation of aryl halides [31, 32]. Moreover, the major disadvantage of catalyst poisoning due to the coordination of cyanide ions to the catalytic metal center was not observe when [$K_4Fe(CN)_6$].$3H_2O$ was used as a cyanating agent [31, 32, 41].

Antimicrobial activity is a term that refers to all active bacteriostatic or bactericidal agents that helps in preventing the growth of bacteria, formation of microbial colonies, and sometimes death of the microorganisms [42]. Nowadays, bacterial infection is one of the most serious clinical concerns, with significant mortality and healthcare costs. Resistance to antibiotics has emerged as a major public health concern with economic and social repercussions globally [43]. The use of NPs has shown broad-spectrum antibacterial activity against both gram-positive and

gram-negative bacteria due to their manageable size of less than 100 nm, which allows them to bond with microbial cells [44]. The biogenically synthesized metal NPs are expected to illustrate improved antibacterial activity through the phytochemical coated metal NPs. Hence, biogenically synthesized metal NPs are emerging as a promising and capable antibacterial agent [45, 46].

In this work, we describe Pd NPs embedded on banana leaves extract-modified graphitic carbon nitride [PdNPs@g-C$_3$N$_4$-BLE] as a nanocatalyst in a continuation of our recent studies of heterogeneous catalysts in Suzuki–Miyaura cross-coupling and cyanation reactions [47–50]. The structure and composition of the PdNPs@g-C$_3$N$_4$-BLE nanocatalyst was examined using several spectroscopic and microscopic techniques. Subsequently, the catalytic activity of PdNPs@g-C$_3$N$_4$-BLE was investigated in Suzuki–Miyaura cross-coupling and aryl halide cyanation reactions. In both the reactions, the PdNPs@g-C$_3$N$_4$-BLE nanocatalyst showed agreeable activity and recyclability up to 12th and 6th recycles respectively. In addition, early in vitro antibacterial testing was performed against the gram-negative bacteria *Escherichia coli* (*E. coli*) and gram-positive bacteria *Bacillus subtilis* (*B. subtilis*). Overall, the biogenically synthesized PdNPs@g-C$_3$N$_4$-BLE nanocatalyst revealed higher catalytic efficiency and antibacterial activity which play significant roles in both industrial and medicinal sectors.

2 Experimental

2.1 Materials

Prior to usage, all solvents were used without any purification. Waste banana leaves were collected from local farmers in the Yadavanahalli region of Bangalore, Karnataka, India. Melamine powder, Pd(OAc)$_2$, [K$_4$Fe(CN)$_6$].3H$_2$O, aryl halides, acids, bases and phenylboronic acids were purchased from Sigma-Aldrich and Avra chemical companies and were used without further purification. Unless otherwise specified, all reactions were carried out in oven-dried glassware with magnetic stirring and heating accomplished by heating mantle or silicone oil bath under aerobic conditions. Thin-layer chromatography (TLC) was used to monitor reactions on 0.25 mm Merck TLC silica gel plates with Ultra-visible (UV) light as a visualizing agent. Column chromatography was performed using silica gel (60–120 mesh, Merck), to purify the reaction products. The removal of volatile solvents with a rotary evaporator attached to a dry diaphragm pump (10–15 mm Hg), followed by pumping to a constant weight with an oil pump (300 mTorr), is referred to as concentration in vacuo.

2.2 Characterization

Fourier transform infrared spectra (FT-IR) were obtained by PerkinElmer spectrometer (L160000A, PerkinElmer, USA). Gas chromatography mass spectroscopy (GC–MS) analysis was performed on Shimadzu (Tokyo, Japan) Make GC–MS-TQ8030 system. The aqueous-ethanolic extract of banana leaves was further extracted using dichloromethane and directly used for GC–MS analysis to know the major phytochemicals present in the banana leaves. By physisorption of N$_2$ gas molecules, Brunauer–Emmett–Teller surface areas (BET) were obtained using BELSORP-max, MicrotracBEL, Japan. Before the analysis, all the samples were degassed at 100 °C for 2 h. UV–Visible spectrophotometer (UV-1900, Shimadzu, Japan) was used to record absorption spectra from the wavelength range of 200–800 nm. Surface morphology along with elemental distribution was analyzed by field emission scanning electron microscopy (FE-SEM) (JEOL JSM-7100F, JEOL, Singapore) with energy dispersive X-ray spectroscopy (EDX), respectively. The total palladium content loaded on the PdNPs@g-C$_3$N$_4$-BLE nanocatalyst was quantified by inductively coupled plasma-optical emission spectroscopy (ICP-OES) (Optima 5300 DV, PerkinElmer, USA). Powder X-ray diffraction measurements (*p*-XRD) were obtained by using Ultima IV X-Ray Diffractometer, Rigaku, Japan. Thermogravimetric/differential thermal analyzer (TGA/DTA) (TGA/DTA Q500 V20.10 Build 36) was employed for thermogravimetric analysis with a heating rate of 10 °C min^{-1} in N$_2$ atmosphere. High resolution transmission electron microscope (HR-TEM) images were obtained by Tecnai G2, T30 S-TWIN (LaB6) (HRTEM 300 kV). Proton nuclear magnetic resonance (^{1}H NMR) spectra were recorded at 400 MHz in deuterated chloroform (CDCl$_3$, δ = 7.26 ppm). ^{1}H NMR coupling constants (*J*) are reported in Hertz (Hz) and multiplicities are specified as follows: s (singlet), d (doublet), t (triplet), m (multiplet).

2.3 Preparation of banana leaves extract (BLE)

Fresh banana leaves were washed with tap water followed by distilled water to remove the impurities present on the surface of the leaves, then fragmented into small pieces and shade dried. The dried leaves were pulverized in an electric blender. Later, 5 g of ground leaves were added into a 250 mL conical flask containing 200 mL of ethanol and distilled water (1:1 v/v) mixture, and stirred for 1 h with a funnel on the mouth of the conical flask. After extraction, the ground leaves were removed by centrifugation of the reaction mixture at 3000 rpm for 5 min. Further the supernatant was filtered to get a clean extract free of extraneous particles. The obtained extract was stored in the refrigerator at 4 °C for further use.

2.4 Synthesis of graphitic carbon nitride (g-C$_3$N$_4$)

In a crucible, 10 g of melamine powder was weighed and placed in a muffle furnace. The temperature of the muffle furnace was raised to 500 °C at a heating rate of 2 °C min^{-1} and maintained for 4 h. The obtained yellow-colored g-C$_3$N$_4$ (4.98 g) was cooled to room temperature for further use [51].

2.5 Synthesis of hydroxyl substituted graphitic carbon nitride (g-C$_3$N$_4$-OH)

In brief, 4 g of prepared g-C$_3$N$_4$ was added to an Erlenmeyer bulb containing a mixture of conc. HNO$_3$ and conc. H$_2$SO$_4$ (1:1 v/v, 20 mL), stirred at room temperature for 2 h, followed by sonication for 30 min. The reaction mass was then centrifuged, rinsed with water until it reached a neutral pH, and successively with ethanol (2×40 mL). The obtained solid was kept overnight for drying at 50 °C to yield the white colored g-C$_3$N$_4$-OH (1.92 g).

2.6 Green synthesis of palladium nanoparticles embedded banana leaves extract-modified graphitic carbon nitride (PdNPs@g-C$_3$N$_4$-BLE)

To an aqueous solution of 100 mL of 10 mM Pd(OAc)$_2$, 0.5 g of g-C$_3$N$_4$-OH was added, sonicated for 20 min and kept for stirring at 85 °C for 1 h. On completion of 1 h, 40 mL of BLE was added drop wise and stirred at the same temperature for 24 h. The reaction mass was then washed with water (2×25 mL) and acetone (2×25 mL). The obtained residue was dried overnight at 50 °C to get an olive green colored PdNPs@g-C$_3$N$_4$-BLE nanocatalyst (0.59 g).

2.7 General procedure for Suzuki–Miyaura cross-coupling reaction

In a round-bottomed flask, PdNPs@g-C$_3$N$_4$-BLE nanocatalyst (2.3 mol% Pd), aryl halide (1.0 equiv.), phenyl boronic acid (1.1 equiv.), and sodium carbonate (2.2 equiv.) were taken. To these, EtOH:H$_2$O (1:1 v/v, 6 mL) was added and stirred at 50 °C for the specified time interval. The progress of the reaction was monitored through TLC. After completion of the reaction, the mixture was cooled to room temperature and the PdNPs@g-C$_3$N$_4$-BLE nanocatalyst was separated by centrifugation. The filtrate was extracted using dichloromethane in a separatory funnel and dried over anhydrous Na$_2$SO$_4$. The dried organic layer was concentrated in vacuo and the product was purified by column chromatography using n-hexane and ethyl acetate as eluents to afford the corresponding products in good to excellent yields. ^{1}H NMR spectra (see supporting information) of all the cross-coupled products were recorded and compared to the standard samples for confirmation.

## 2.8 General procedure for cyanation of aryl halides

A solution of aryl halide (1 equiv.), K$_4$[Fe(CN)$_6$].3H$_2$O (0.17 equiv., as the cyanide source), Na$_2$CO$_3$ (1.5 equiv.), and PdNPs@g-C$_3$N$_4$-BLE nanocatalyst (2.3 mol% Pd) in DMF (5 mL) was magnetically swirled at 140 °C for the required time period. On completion of the reaction, as determined by TLC, the reaction mixture was cooled to room temperature and centrifuged at 3000 rpm for 15 min to separate the PdNPs@g-C$_3$N$_4$-BLE nanocatalyst. The obtained supernatant was then extracted with ethyl acetate, washed with water (2×20 mL) and the organic phase was dried over anhydrous Na$_2$SO$_4$. The dried organic layer was concentrated in vacuo and the product was purified through column chromatography using n-hexane and ethyl acetate as eluents to afford the corresponding products in good to excellent yields. All the aryl nitrile products were known molecules and were confirmed by comparing ^{1}H NMR data with standard samples (see supporting information).

2.9 General procedure for antimicrobial activity

The agar well diffusion method with 4 circular wells (6 mm) and sterile borer was used to screen the antimicrobial activity of the g-C$_3$N$_4$ and PdNPs@g-C$_3$N$_4$-BLE nanocatalyst. For this, E. coli and B. subtilis were used as test organisms and were inoculated overnight in bacteriological incubator at 37 ºC. The test organisms were then loaded with the help of L-shaped glass spreader across the petri plate having solidified nutrient agar using the spread plate technique. The g-C$_3$N$_4$ and PdNPs@g-C$_3$N$_4$-BLE nanocatalyst were loaded on different plates along with standard streptomycin (10 µg), and the vehicles used for streptomycin (distilled water) and for g-C$_3$N$_4$ and PdNPs@g-C$_3$N$_4$-BLE nanocatalyst (ethylene glycol:HCl (9:1)). The plates were then incubated for 24 h at 37 ºC and the results were analyzed and recorded. The analysis was carried out in triplicates, and the average of the three was taken.

2.10 Procedure for recovery of the PdNPs@g-C$_3$N$_4$-BLE nanocatalyst

In organic transformations, the catalyst's stability and reusability are significant considerations, especially for practical industrial applications. To address this, the separated PdNPs@g-C$_3$N$_4$-BLE nanocatalyst, following reaction completion, was washed with water (2×20 mL), methanol (2×20 mL), and dried at 45 °C for 12 h. The dried PdNPs@g-C$_3$N$_4$-BLE nanocatalyst was employed as such for the next round of reaction.
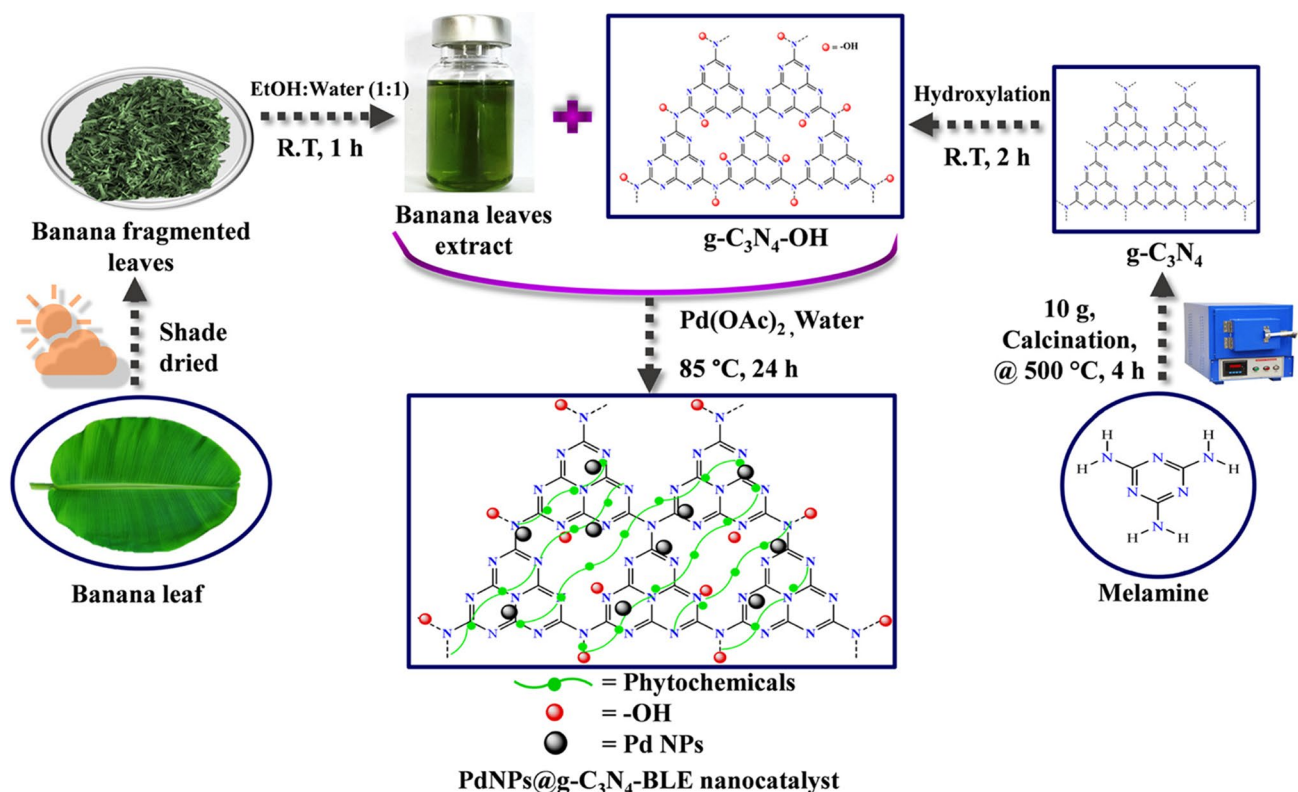
Scheme 1 Synthetic scheme for the preparation of PdNPs@g-C$_3$N$_4$-BLE nanocatalyst

3 Results and discussion

3.1 Synthesis of PdNPs@g-C$_3$N$_4$-BLE nanocatalyst

We report here the synthesis of PdNPs@g-C$_3$N$_4$-BLE nanocatalyst from melamine and aqueous-ethanolic extract of banana leaves, without the use of any hazardous or harmful chemicals or solvents as illustrated in Scheme 1. Banana leaves were chosen for the study due to their plenitude and presence of considerable number of phytochemicals containing phenols, acids, terpenoids, tannins, etc. [13]. These phytochemicals aid in the reduction of Pd(II) to Pd(0), as well as the variety of functional groups available in them help in retaining Pd NPs adhered to the support. Firstly, g-C$_3$N$_4$ was prepared from the nitrogen rich triazine compound melamine through polymerization of tri-*s*-triazine by calcination at 500 °C for 4 h. The surface of g-C$_3$N$_4$ was then hydroxylated to increase its surface hydroxyl group by treating it with conc. HNO$_3$ and conc. H$_2$SO$_4$ (1:1v/v) at room temperature for 2 h. This assists in activating the g-C$_3$N$_4$ surface for better binding to the phytochemicals. Lastly, Pd(OAc)$_2$ dispersed in an aqueous solution of g-C$_3$N$_4$-OH by constant stirring for 1 h at 85 °C was treated with BLE and further stirred for 24 h. The BLE itself plays the important roles of capping, stabilizing and reducing agent, usually used in nanoparticle synthesis, enabling three-in-one property for

the formation of stable Pd NPs. In the desired PdNPs@g-C$_3$N$_4$-BLE nanocatalyst, obtained as olive green colored solid, the phytochemicals in the banana leaves extract and the hydroxyl groups on the heterogeneous support will serve as securing points for the Pd NPs.

3.2 Spectroscopic and microscopic characterization

3.2.1 FT-IR spectroscopy

FT-IR spectroscopy was performed to evaluate the change in chemical composition from g-C$_3$N$_4$ to PdNPs@g-C$_3$N$_4$-BLE nanocatalyst (Fig. 1). In the FT-IR spectrum of g-C$_3$N$_4$ (Fig. 1a), peaks observed at 807 cm^{-1} is assigned to the out-of-plane vibration characteristic of C-N heterocycles. Several bands from 1239 to 1643 cm^{-1} are due to the 1,3,5-triazine units. The broad band at 3165 cm^{-1} represents the presence of the -NH$_2$ group [52]. In the FT-IR spectrum of g-C$_3$N$_4$-OH (Fig. 1b) the peaks of g-C$_3$N$_4$ are retained and the absorption peaks observed at 2426, 2135, and 1114 cm^{-1} are due to the vibrations of the terminal nitrile group and the oxygen containing groups. The peak located at 3350 cm^{-1} is merged with 3150 cm^{-1} mainly due to the overlapping of the stretching vibrations of -OH groups with –NH$_2$ groups [53]. The FT-IR spectrum of BLE (Fig. 1c) exhibited the stretching vibration of -OH group at 3400 cm^{-1}, asymmetric
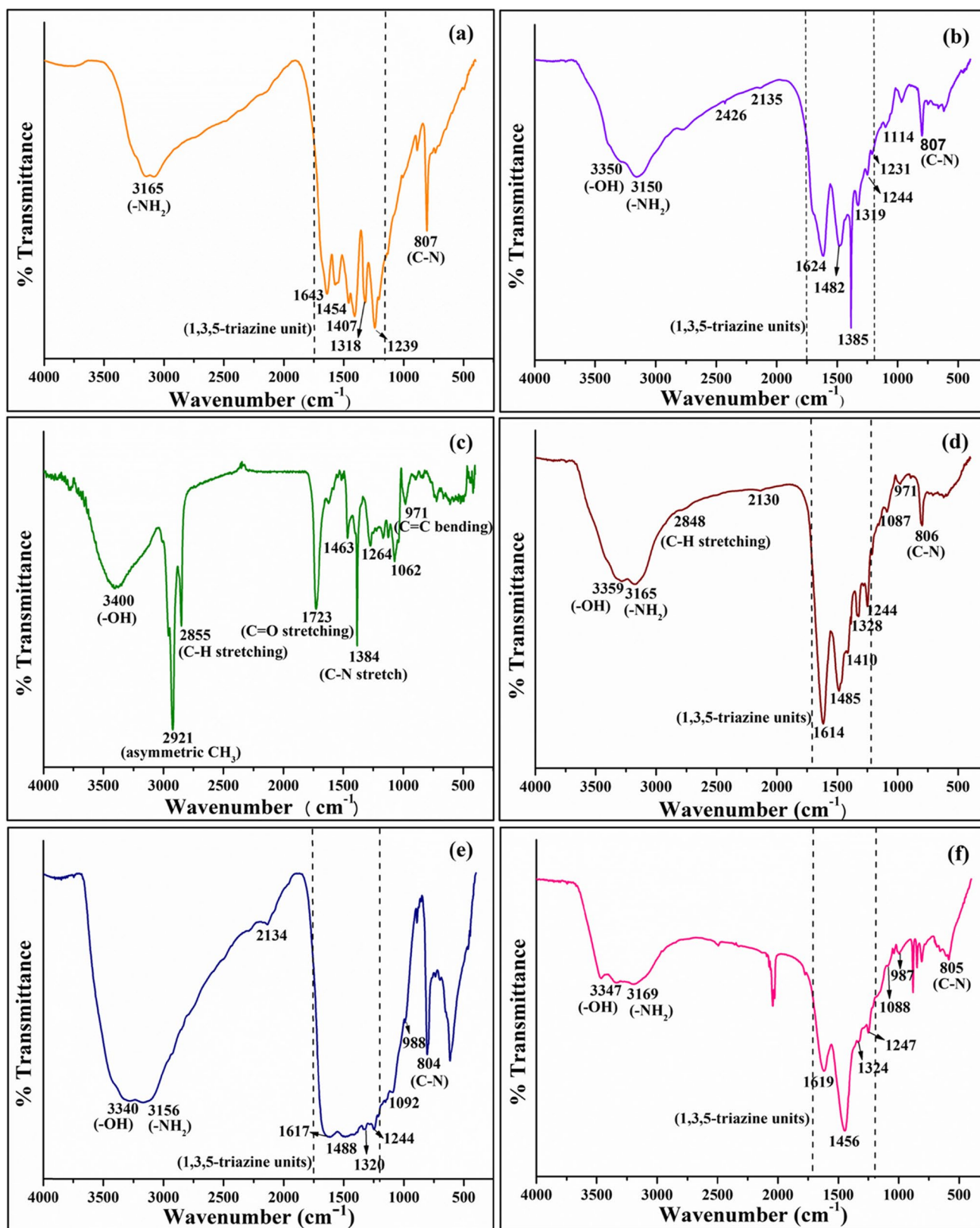
Fig. 1 FT-IR spectra of (**a**) g-C_3N_4, (**b**) g-C_3N_4-OH, (**c**) BLE, (**d**) fresh PdNPs@g-C_3N_4-BLE nanocatalyst, (**e**) twelve times recycled PdNPs@g-C_3N_4-BLE nanocatalyst used for Suzuki–Miyaura cross-coupling, and (**f**) six times recycled PdNPs@g-C_3N_4-BLE nanocatalyst used for aryl halide cyanation

stretching of a methyl group at 2921 cm^{-1}, C-H stretching of alkanes and/or secondary amine at 2855 cm^{-1}, C=O stretching at 1723 cm^{-1}, -NH stretching vibration at 1463 cm^{-1}, and aromatic amines (C-N stretching) at 1384 cm^{-1}, and the peaks at 1264 cm^{-1}, 1062 cm^{-1}, and 971 cm^{-1} indicate the presence of alcohols, carboxylic acids, and C=C bending of alkenes respectively. These peaks indicate the existence of active constituents such as saponins, phenols, terpenoids, steroids and tannins which are responsible for the reduction of Pd(II) to Pd(0), as well as for stabilization of Pd(0) on g-C$_3$N$_4$-OH. Furthermore, in the FT-IR spectrum of PdNPs@g-C$_3$N$_4$-BLE nanocatalyst (Fig. 1d), presence of peaks corresponding to the stretching vibrations of functional groups present in BLE, g-C$_3$N$_4$ and -OH groups, indicate the successful coating of phytochemicals and formation of Pd NPs onto g-C$_3$N$_4$-OH. The FT-IR spectra of the recycled PdNPs@g-C$_3$N$_4$-BLE nanocatalyst in Suzuki–Miyaura cross-coupling and aryl halide cyanation reactions remained basically intact with minor variations in the peaks aside from the merging of peaks in the range 1617–1244 cm^{-1} (Fig. 1e and f), confirming the retention of the chemical structure.

3.2.2 p-XRD analysis

In each step, p-XRD patterns were recorded to analyze the structural modifications (Fig. 2). The two diffraction peaks of g-C$_3$N$_4$ at 2θ=12.30° and 27.56° correspond to the (100) and (002) planes (Fig. 2a, JCPDS card No. 85–1526). The diffraction pattern of g-C$_3$N$_4$-OH (Fig. 2b) was found to preserve the crystal structure of g-C$_3$N$_4$ even after functionalization. The PdNPs@g-C$_3$N$_4$-BLE nanocatalyst showed
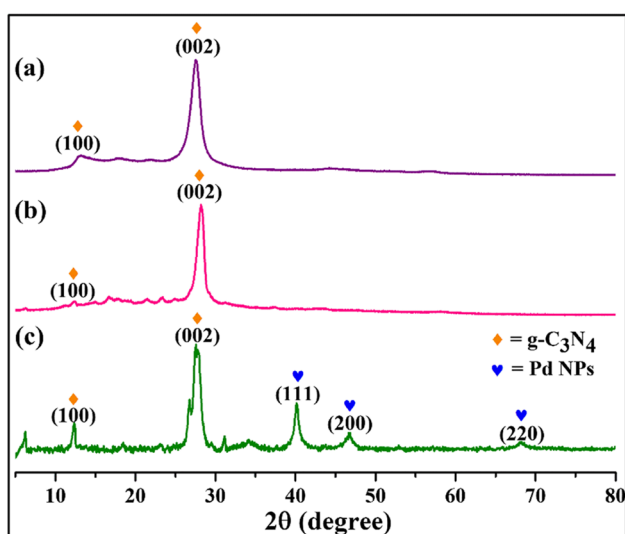
three additional diffraction peaks at 2θ=40.24°, 46.51° and 68.04° corresponding to the (111), (200) and (220) planes of Pd NPs respectively (Fig. 2c, JCPDS card No. 05–0681). From the lattice planes, it confirms the presence of face centered cubic crystal structure of Pd NPS in the PdNPs@g-C$_3$N$_4$-BLE nanocatalyst which matches well with reported literature. In addition, the Debye–Scherrer formula was used to calculate the average crystallite size of Pd NPs in the PdNPs@g-C$_3$N$_4$-BLE nanocatalyst, which was found to be 14.98 nm.

3.2.3 GC–MS analysis of BLE

GC–MS analysis of the aqueous-ethanolic extract of banana leaves (Table 1) indicated the presence of major phytochemical components such as phenols, acids, terpenoids, tannins like 2,4-di-tert-butylphenol, 1-nonadecene, 1,2-benzenedicarboxylic acid, bis(2-methylpropyl) ester, bis(2-ethylhexyl) phthalate, 1-heptacosanol and dibutyl phthalate which are responsible for the reduction of Pd(II) to Pd(0) and stabilization of the PdNPs@g-C$_3$N$_4$-BLE nanocatalyst.

3.2.4 Qualitative analysis of phytochemicals present in BLE

Qualitative analysis was carried out to identify the phytochemicals present in the aqueous-ethanolic banana leaves extract. The results of the color reactions are shown in Fig. 3. The results of the various tests conducted for saponins, phenols, steroids, terpenoids, and tannins were well-matched with the literature reports [54, 55] and are summarized in Table S1.
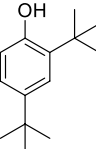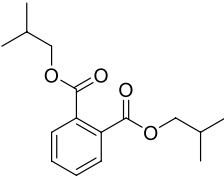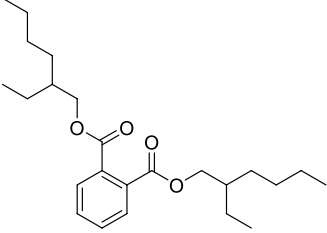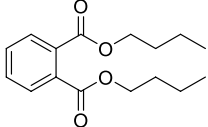
3.2.5 ICP-OES analysis

The exact quantity of palladium present in the PdNPs@g-C$_3$N$_4$-BLE nanocatalyst was quantified by ICP-OES analysis. The palladium loading on the PdNPs@g-C$_3$N$_4$-BLE nanocatalyst was found to be 12.21% w/w.

3.2.6 TG/DTA analysis

For catalysts to maintain their activity over a wider range of reaction temperature and durations, thermal stability is a crucial feature. Thermally stable catalysts are particularly significant for industrial applications that need extensive thermal treatment. Thus, the thermal stability of g-C$_3$N$_4$ and the PdNPs@g-C$_3$N$_4$-BLE nanocatalyst was estimated by TG/DTA analysis at a heating rate of 10 °C min^{-1} under a nitrogen atmosphere between 40 °C and 800 °C (Fig. 4). The g-C$_3$N$_4$ remained stable up to 550 °C, followed by a sudden weight loss of about ∼99% in the range of 570–700 °C, which may be due to the disintegration of the tri-s-triazine units of g-C$_3$N$_4$ (Fig. 4a). The oxidation

Fig. 2 p-XRD patterns of (**a**) g-C$_3$N$_4$, (**b**) g-C$_3$N$_4$-OH, and (**c**) PdNPs@g-C$_3$N$_4$-BLE nanocatalyst

Table 1 Phytochemicals identification using GC–MS

Sl. No.	RT	Area (%)	Structure	Name of the compound
1.	7.38	7.86		2,4-Di-tert-butylphenol
2.	8.48	3.62		1-Nonadecene
3.	8.76	29.49		1,2-Benzenedicarboxylic acid, bis(2-methylpropyl) ester
4.	10.89	30.10		Bis(2-ethylhexyl)phthalate
5.	9.80	4.07		1-Heptacosanol
6.	8.92	5.67		Dibutyl phthalate

of g-C_3N_4 to produce CO_2 and NH_3 may be responsible for the exothermic peak [56] around 670 °C as observed in the DTA curve (Fig. 4a). On the other hand, the TG curve of the PdNPs@g-C_3N_4-BLE nanocatalyst is shown in Fig. 4b. The PdNPs@g-C_3N_4-BLE nanocatalyst was observed to degrade in three stages. In the first stage, ~10% weight loss found in the range of 50–115 °C corresponds to the evaporation of adsorbed water molecules as well as volatile organic moieties. The second stage occurred from 180 to 330 °C, with ~21% weight loss due to the evaporation/degradation of bare phytochemicals and loss of -OH groups. The highest deterioration was observed in the third stage, between 550 and 600 °C with a weight loss of ~60%. This is due to the complete disintegration of tri-s-triazine units of g-C_3N_4. Furthermore, the DTA curve showed two broad exothermic peaks at 254 °C and from 500 °C corresponding to the degradation of -OH groups and phytochemicals grafted on PdNPs@g-C_3N_4-BLE nanocatalyst (Fig. 4b). Based on TG/DTA curve, it can be concluded that the PdNPs@g-C_3N_4-BLE nanocatalyst is stable up to 200 °C, allowing it to be employed in organic transformations up to 200 °C.

3.2.7 UV–visible analysis

UV–visible spectroscopy was applied to check the utilization of phytochemicals during the synthesis process. The absorption spectrum of the fresh BLE exhibited two λ_{max} at wavelengths 260 and 350 nm (Fig. 5a) that are responsible for the presence of polyphenolic tannin and other phytocomponents. The absorption spectrum of the extract after Pd(II)–Pd(0) reduction showed decrease in the intensity of the absorption peaks in comparison to the fresh extract (Fig. 5b). Thus, it has been concluded that the phytochemicals found in BLE are successfully utilized in the synthesis of PdNPs@g-C_3N_4-BLE nanocatalyst.

3.2.8 FE-SEM and EDX analysis

FE-SEM analysis was performed to obtain information about the surface morphology of synthesized g-C_3N_4, g-C_3N_4-OH and PdNPs@g-C_3N_4-BLE nanocatalyst (Fig. 6). It was observed that the g-C_3N_4 is made up of number of nanosheets and some worm-like nano vessels formed by the
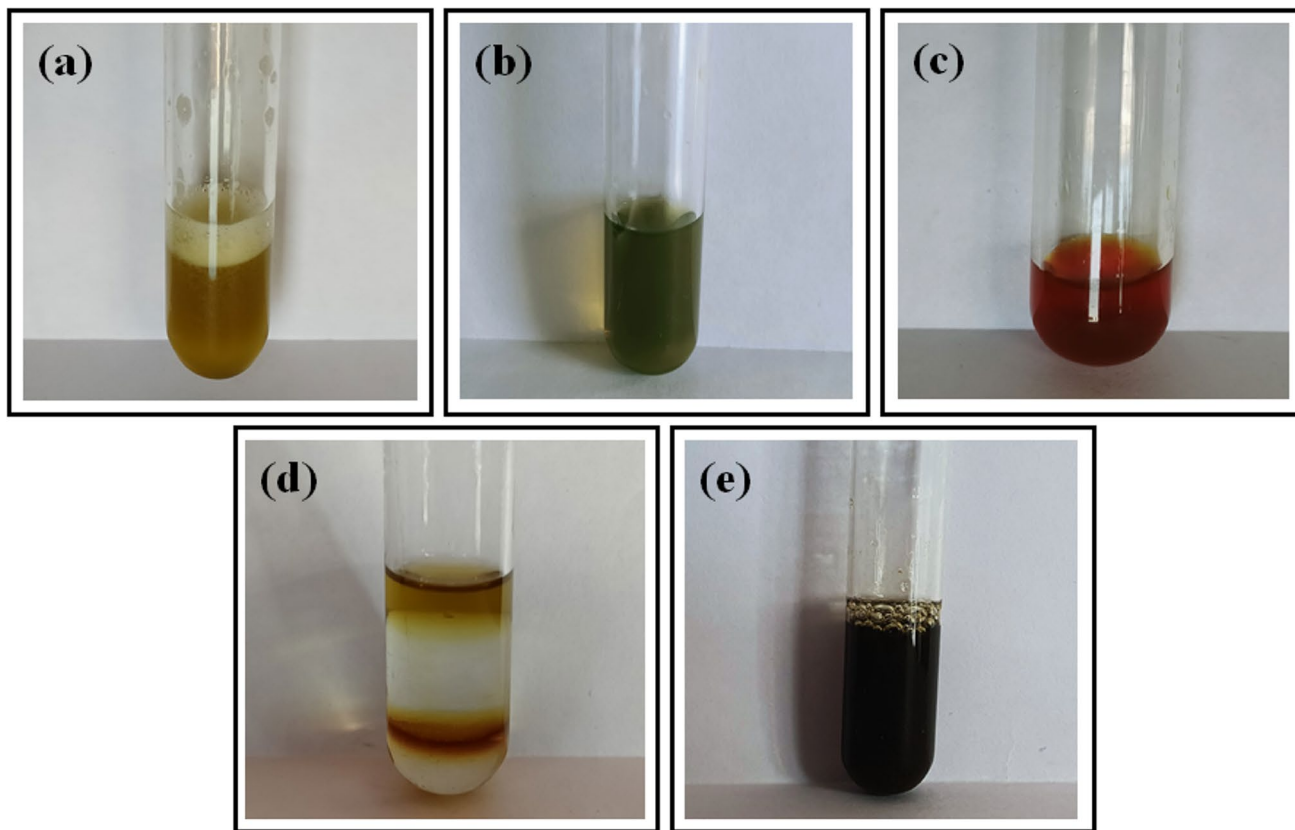
Fig. 3 Images of results of qualitative tests for (**a**) saponins, (**b**) phenols, (**c**) steroids, (**d**) terpenoids, and (**e**) tannins
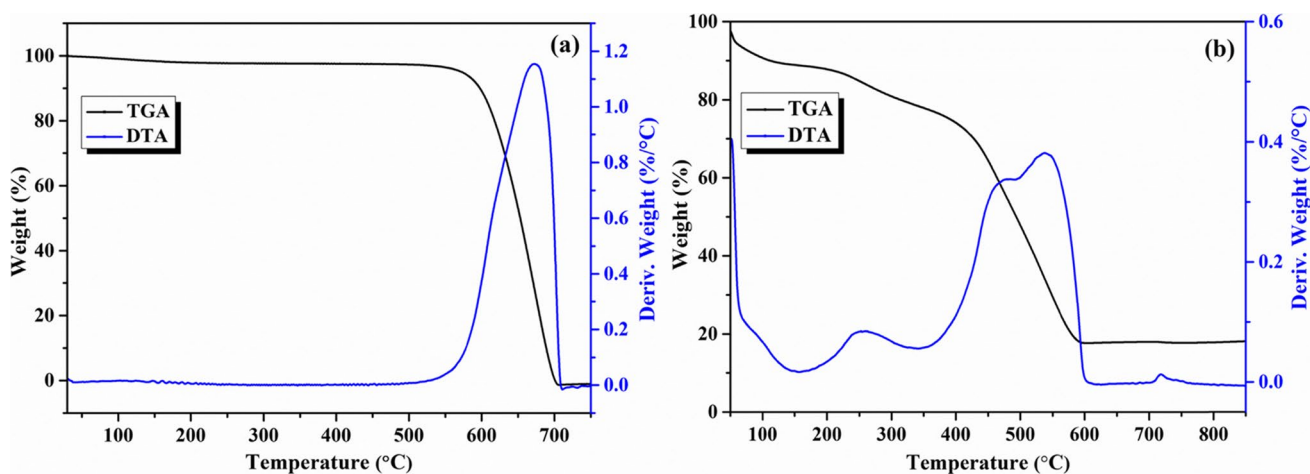

Fig. 4 TG/DTA curve of (**a**) g-C$_3$N$_4$ and (**b**) PdNPs@g-C$_3$N$_4$-BLE nanocatalyst

curling of the nanosheets (Fig. 6a). The unequal temperature distribution during calcination may be the cause of the non-uniform morphology of the g-C$_3$N$_4$ [56]. Exfoliation of the g-C$_3$N$_4$ during the formation of g-C$_3$N$_4$-OH caused some of the worm-like structure to break and form sheet-like morphologies as seen in Fig. 6b. From the FE-SEM

image of PdNPs@g-C$_3$N$_4$-BLE nanocatalyst (Fig. 6c), we may deduce that the small spherical particles accumulated on the layer of g-C$_3$N$_4$-OH could represent the biologically synthesized Pd NPs. The surface morphology of the 12 times and 6 times recycled PdNPs@g-C$_3$N$_4$-BLE nanocatalyst used in Suzuki–Miyaura cross-coupling and aryl halide
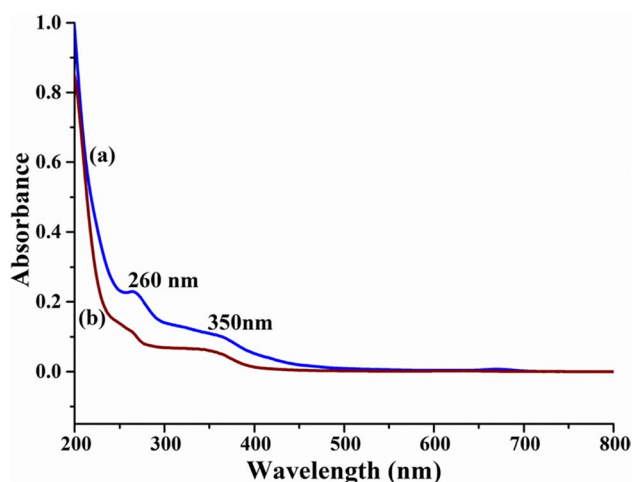
Fig. 5 UV–visible spectra of (**a**) fresh extract and (**b**) extract after reduction

cyanation reactions, respectively, remained substantially identical to that of the fresh PdNPs@g-C_3N_4-BLE nanocatalyst (Fig. 6d and e). However, an increase in agglomeration was observed after 6 times recycled PdNPs@g-C_3N_4-BLE nanocatalyst used in cyanation reaction (Fig. 6e). From the EDX analysis the elemental composition of the biogenically synthesized PdNPs@g-C_3N_4-BLE nanocatalyst was confirmed. The EDX spectrum (Fig. S1) revealed the presence

of C, N, O, and Pd, which represents the successful grafting of Pd on the surface of BLE modified g-C_3N_4. The elemental mapping of the PdNPs@g-C_3N_4-BLE nanocatalyst showed the distribution of elements to be uniform (Fig. S2).

3.2.9 HR-TEM analysis

Furthermore, HR-TEM analysis was carried out to substantiate the surface morphology of the g-C_3N_4 and PdNPs@g-C_3N_4-BLE nanocatalyst obtained from FE-SEM analysis. The HR-TEM image of g-C_3N_4 showed curled worm-like structure embodied in a strip-like nanosheet, which is consistent with the FE-SEM image (Fig. 7a). In the HR-TEM image of the PdNPs@g-C_3N_4-BLE nanocatalyst, the immobilization of Pd NPs on the g-C_3N_4 sheet is clearly visible as black spots as seen in Fig. 7b. The (111) diffraction plane of Pd NPs in the PdNPs@g-C_3N_4-BLE nanocatalyst showed the planar spacing of the atomic lattice fringes of 0.22 nm (Fig. 7c). The selected area electron diffraction (SAED) pattern of the PdNPs@g-C_3N_4-BLE nanocatalyst displayed polycrystalline nature (Fig. 7d). Furthermore, from the particle size distribution, particle size was observed to vary from 4 to 18 nm with an average diameter of 8.8 nm (Fig. 7e). The elemental mapping of the PdNPs@g-C_3N_4-BLE nanocatalyst (Fig. 7f–i) was also in agreement with that of Fig. S2.
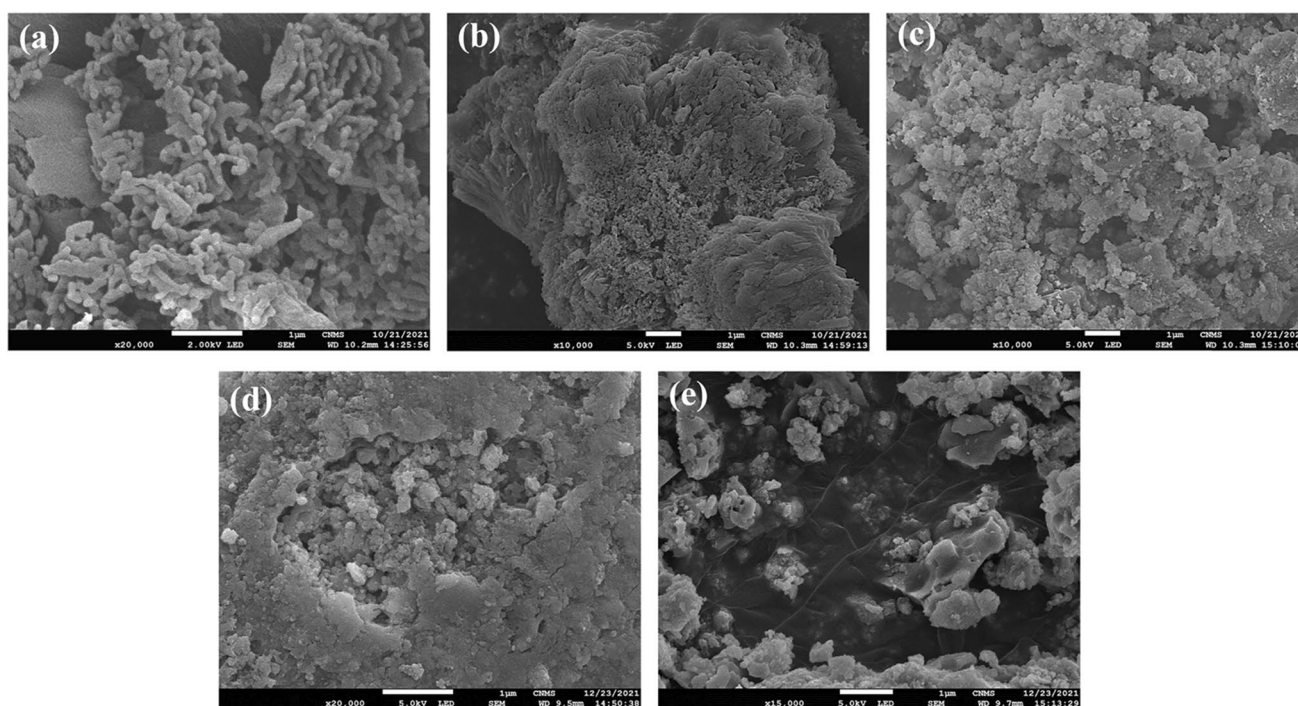
Fig. 6 FE-SEM images of (**a**) g-C_3N_4, (**b**) g-C_3N_4-OH, (**c**) fresh PdNPs@g-C_3N_4-BLE nanocatalyst, (**d**) twelve-times recycled PdNPs@g-C_3N_4-BLE nanocatalyst used in Suzuki–Miyaura cross-coupling, and (**e**) six-times recycled PdNPs@g-C_3N_4-BLE nanocatalyst used in cyanation reaction
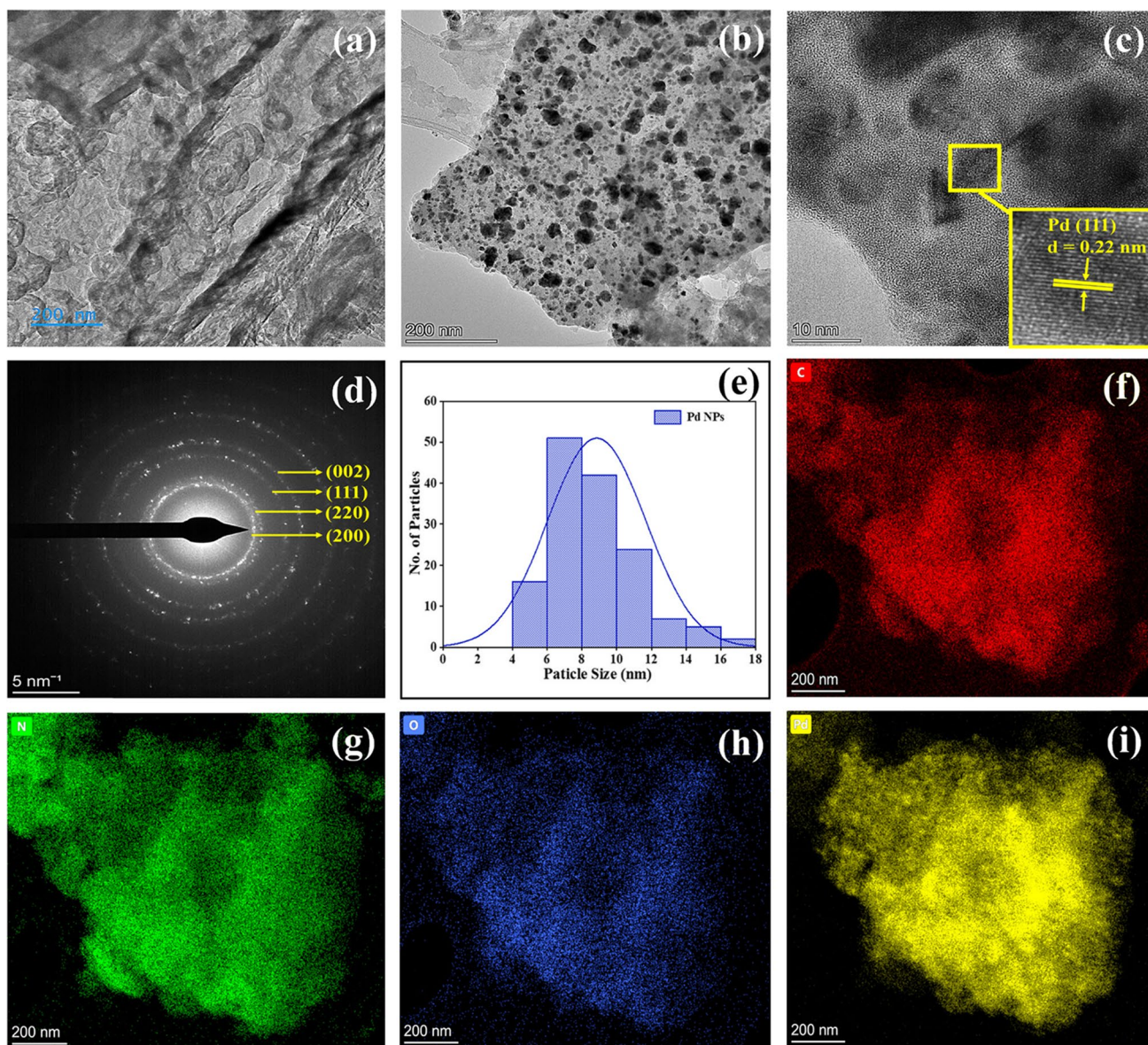
Fig. 7 HR-TEM images of (**a**) g-C$_3$N$_4$, (**b**) PdNPs@g-C$_3$N$_4$-BLE nanocatalyst and the corresponding (**c**) palladium d-spacing, (**d**) SAED pattern, (**e**) average particle size distribution, and (**f–i**) elemental mapping

3.2.10 BET surface area analysis

To calculate the specific surface area of g-C$_3$N$_4$, g-C$_3$N$_4$-OH, and PdNPs@g-C$_3$N$_4$-BLE nanocatalyst, the BET analysis was employed. The nitrogen adsorption–desorption curves for g-C$_3$N$_4$, g-C$_3$N$_4$-OH, and PdNPs@g-C$_3$N$_4$-BLE nanocatalyst showed type II isotherm (Fig. 8) indicating the presence of mesoporous structure. The g-C$_3$N$_4$ has a small specific surface area of 9.85 m^2 g^{-1} (Fig. 8a), however, due to exfoliation the g-C$_3$N$_4$-OH showed a specific surface area of 26.92 m^{2}g^1 (Fig. 8b) [57]. Furthermore, the specific surface area of the PdNPs@g-C$_3$N$_4$-BLE nanocatalyst was found to be 55.85 m^2 g^{-1} (Fig. 8c), which could be related

to the presence of phytochemicals. From the BJH pore size distribution plot, the mean pore diameter and mean pore volume of PdNPs@g-C$_3$N$_4$-BLE nanocatalyst were obtained as 7.01 nm and 0.098 cm^3 g^{-1}, respectively (Fig. 8d).

3.3 Catalytic activity of PdNPs@g-C$_3$N$_4$-BLE in Suzuki–Miyaura cross-coupling reaction

Following a comprehensive assessment using a variety of analytical techniques, the air and moisture stable PdNPs@g-C$_3$N$_4$-BLE nanocatalyst was evaluated for its catalytic potential in Suzuki–Miyaura cross-coupling reaction. The Suzuki–Miyaura cross-coupling
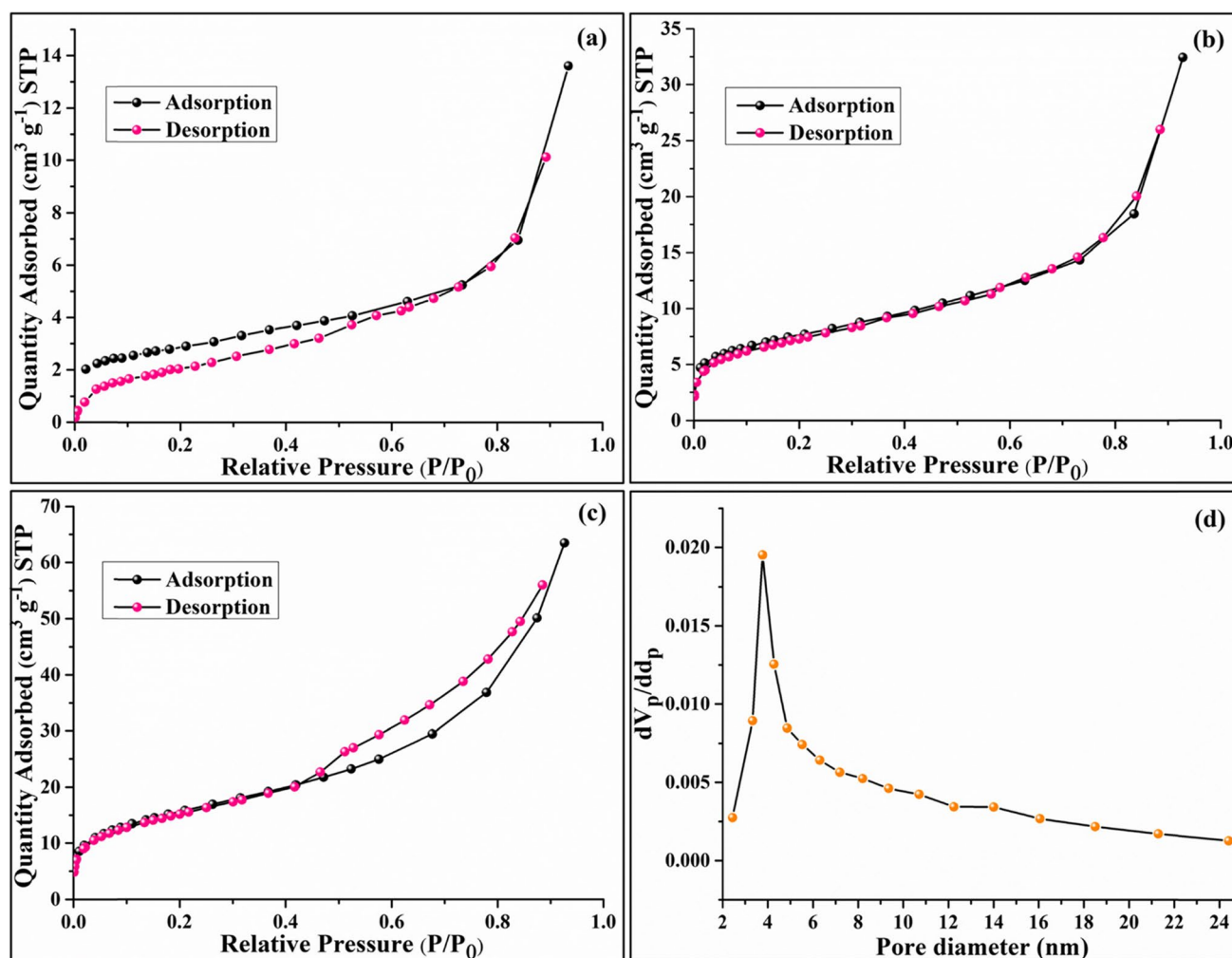
Fig. 8 Nitrogen adsorption–desorption curves for (**a**) g-C$_3$N$_4$, (**b**) g-C$_3$N$_4$-OH, (**c**) PdNPs@g-C$_3$N$_4$-BLE nanocatalyst, and (**d**) BJH pore size distribution plot of PdNPs@g-C$_3$N$_4$-BLE nanocatalyst

reaction is particularly interesting in the synthesis of biaryls and derivatives by C–C bond formation. As illustrated in Scheme 2, the reaction conditions for a model Suzuki–Miyaura cross-coupling reaction of 4-iodoanisole with phenylboronic acid were optimized. In this study we have mainly focused on cost-effective and environmentally friendly synthetic routes. As a result, during optimization, green solvents such as ethanol and water were prioritized. The early results showed that utilizing Na$_2$CO$_3$ as the base, EtOH:H$_2$O (1:1 v/v) as the solvent, and 2.3 mol% PdNPs@g-C$_3$N$_4$-BLE nanocatalyst at 50 °C in 2 h yielded

the best yield and hence considered as the optimized conditions (Table 2, entry 5).

Table 2 summarizes the impact of several parameters such as solvent, base, time, and catalyst loading on the performance of the PdNPs@g-C$_3$N$_4$-BLE nanocatalyst for the model reaction for Suzuki–Miyaura cross-coupling reaction. The role of catalyst ratio in organic transformation is very important. As a result, we have studied the influence of the nanocatalyst by varying catalyst loading. Typically, 0.6, 1.2, 2.3, 3.5 and 4.6 mol% of Pd (Table 2, entries 3–7) were used to determine the optimum amount
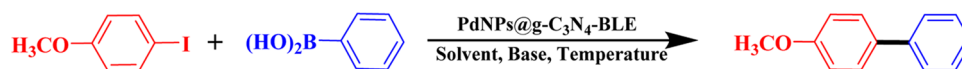
Scheme 2 Suzuki–Miyaura cross-coupling reaction between 4-iodoanisole with phenylboronic acid in the presence of the PdNPs@g-C$_3$N$_4$-BLE nanocatalyst

Table 2 Optimization of reaction conditions for Suzuki–Miyaura cross-coupling reaction of 4-iodoanisole with phenylboronic acid[a]

Entry	Base	Solvent	Temp. (°C)	Pd (mol%)	Time (h)	Yield[b] (%)
1	Na_2CO_3	$EtOH:H_2O$ (1:1)	RT	2.3	2	45
2	Na_2CO_3	$EtOH:H_2O$ (1:1)	RT	2.3	2.6	52
3	Na_2CO_3	$EtOH:H_2O$ (1:1)	50	0.6	2	42
4	Na_2CO_3	$EtOH:H_2O$ (1:1)	50	1.2	2	74
5	**Na_2CO_3**	**$EtOH:H_2O$ (1:1)**	**50**	**2.3**	**2**	**98**
6	Na_2CO_3	$EtOH:H_2O$ (1:1)	50	3.5	2	92
7	Na_2CO_3	$EtOH:H_2O$ (1:1)	50	4.6	2	92
8	Na_2CO_3	$EtOH:H_2O$ (1:1)	60	2.3	2	98
9	Na_2CO_3	$EtOH:H_2O$ (1:1)	50	-	2	-
10	Na_2CO_3	Water	50	2.3	2	22
11	Na_2CO_3	EtOH	50	2.3	2	45
12	Na_2CO_3	MeOH	50	2.3	2	40
13	Na_2CO_3	DMF	50	2.3	2	NR
14	Na_2CO_3	Acetonitrile	50	2.3	2	NR
15	Na_2CO_3	1,4-Dioxane	50	2.3	2	NR
16	K_2CO_3	$EtOH:H_2O$ (1:1)	50	2.3	2	92
17	NaOH	$EtOH:H_2O$ (1:1)	50	2.3	2	42
18	KOH	$EtOH:H_2O$ (1:1)	50	2.3	2	48
19	KF	$EtOH:H_2O$ (1:1)	50	2.3	2	45
20	$Na_3PO_4.12H_2O$	$EtOH:H_2O$ (1:1)	50	2.3	2	86
21	Et_3N	$EtOH:H_2O$ (1:1)	50	2.3	2	88
22	Cs_2CO_3	$EtOH:H_2O$ (1:1)	50	2.3	2	85

Bold value indicates the best reaction condition among the sets of reactions performed

[a]Reaction conditions: 4-iodoanisole (1 equiv.), phenylboronic acid (1.1 equiv.), PdNPs@g-C$_3$N$_4$-BLE (mol% palladium with respect to aryl halide), base (2.2 equiv.), and solvent (6 mL) in air

[b]Isolated yield after separation by column chromatography; average of two runs

of the PdNPs@g-C$_3$N$_4$-BLE nanocatalyst required for the reaction and the products were obtained in 42, 74, 98, 92, and 92% yields, respectively. When 2.3 mol % of Pd was utilized (Table 2, entry 5), the best yield of 98% was produced, and further increase in the catalyst ratio did not increase the yield (Table 2, entries 6 and 7). Furthermore, to investigate the role of the nanocatalyst in cross-coupling reactions, a control experiment was carried out without the PdNPs@g-C$_3$N$_4$-BLE nanocatalyst, and no cross-coupled product was observed (Table 2, entry 9), signifying the requirement of the nanocatalyst. Different solvents such as H$_2$O, EtOH:H$_2$O (1:1), EtOH, MeOH, DMF, acetonitrile, and 1,4-dioxane were used to test the effect of solvent on the catalytic potential of the PdNPs@g-C$_3$N$_4$-BLE nanocatalyst. The reaction proceeded well with polar protic solvents such as H$_2$O, EtOH:H$_2$O (1:1), EtOH, and MeOH (Table 2, entries 10, 5, 11, and 12), while this was not seen with polar aprotic solvents such as DMF, acetonitrile, and 1,4-dioxane (Table 2, entries 13–15). This could be due to the poor solubility of the reagents in these solvents as reported in various data bases [58]. Among the solvent systems tested, EtOH:H$_2$O (1:1) mixture gave the best

yield (Table 2, entry 5) where both the reactants and the base is highly soluble and hence shows the excellent catalytic activity with high yield compared to other solvents. Furthermore, the effect of base on the catalytic activity of the PdNPs@g-C$_3$N$_4$-BLE nanocatalyst was investigated using the following bases: Na$_2$CO$_3$, K$_2$CO$_3$, NaOH, KOH, KF, Na$_3$PO$_4$.12H$_2$O, Et$_3$N (triethylamine), and Cs$_2$CO$_3$ (Table 2, entries 5 and 16–22). The bases Na$_2$CO$_3$, K$_2$CO$_3$, Na$_3$PO$_4$.12H$_2$O, Et$_3$N, and Cs$_2$CO$_3$ showed good to excellent yields (Table 2, entries 5, 16, and 20–22). On the other hand, NaOH, KOH, and KF showed reduced conversion (Table 2, entries 17–19). In comparison to other bases, Na$_2$CO$_3$ is cheap and non-toxic, which also furnished the highest yield (Table 2, entry 5). Therefore, Na$_2$CO$_3$ was selected as the base for further reactions. The influence of temperature on the catalytic activity of the PdNPs@g-C$_3$N$_4$-BLE nanocatalyst was investigated at room temperature, 50 and 60 °C. The rate of catalytic activity increased with increase in temperature from room temperature to 50 °C beyond which the yield remained constant (Table 2, entries 2, 5, 8). Hence the reaction temperature was optimized as 50 °C (Table 2, entry 5). The model reaction was carried out at various time intervals

using the PdNPs@g-C₃N₄-BLE nanocatalyst to explore the influence of time (Table 2). As a result, the optimum period for the cross-coupled products was determined to be 2 h.

3.3.1 Suzuki–Miyaura cross-coupling reaction between different aryl halides with aryl boronic acids using PdNPs@g-C₃N₄-BLE nanocatalyst

A wide range of electron-donating (-OCH₃, -CH₃, -OH) and electron-withdrawing (-NO₂, -CN, -COCH₃, and -CHO) groups substituted aryl halides (-I, -Br, -Cl) were cross-coupled with different phenylboronic acids (phenyl, 4-chlorophenyl, and 4-carboxyphenyl boronic acids) under optimized reaction conditions to study the scope and general applicability of the PdNPs@g-C₃N₄-BLE nanocatalyst in Suzuki–Miyaura cross-coupling reaction. The results are summarized in Table 3. The results demonstrate that aryl iodides gave good to exceptional yields compared to aryl bromides which was better than that of aryl chlorides (Table 3, entries 1–4, 6, 7, 12, 13, 15–19). Although the electronic properties of the substituents had little effect on product formation, steric interactions impeded the cross-coupling reaction as seen in –OCH₃ and CHO groups substituted at 2- and 4-positions of the aryl halide (Table 3, entries 1, 5, 10, and 11). Likewise, on substituting the 4-position of phenylboronic acid with electron withdrawing groups such as –Cl and –COOH, decrease in the conversion was observed compared to the unsubstituted acid (Table 3, entries 1–4, 17–19). The PdNPs@g-C₃N₄-BLE nanocatalyst demonstrated high selectivity towards the formation of the cross-coupled products with high TONs and TOFs, while only trace amounts of the biphenyl homo-coupled product was observed, thus, indicating the PdNPs@g-C₃N₄-BLE nanocatalyst to be very selective. To broaden the applicability of the PdNPs@g-C₃N₄-BLE nanocatalyst, we have synthesized a non-steroidal anti-inflammatory drug (NSAID) Felbinac [59], which relieves muscular aches and pains, as well as discomfort due to sprains and strains. Felbinac was synthesized using green reaction conditions in 2 h through Suzuki–Miyaura cross-coupling of 4-bromophenylacetic acid with phenylboronic acid (Table 3, entry 21).

The plausible mechanism involved in Suzuki–Miyaura cross-coupling reaction using PdNPs@g-C₃N₄-BLE nanocatalyst is depicted in Scheme 3. The C–C cross-coupled products are obtained via the possible mechanistic intermediates (**II** and **III**). Firstly, the oxidative addition of the aryl halide onto the nanocatalyst to form **II**. Secondly, the transmetallation between **II** and the base activated arylboronic acid to give **III**, which undergoes reductive

elimination to yield the cross-coupled product and the nanocatalyst.

3.3.2 Recyclability of the PdNPs@g-C₃N₄-BLE nanocatalyst in Suzuki–Miyaura cross-coupling reaction

The recycling of catalysts is necessary from the economic and environmental points of view. Therefore, recyclability study of the PdNPs@g-C₃N₄-BLE nanocatalyst was investigated by using the Suzuki–Miyaura cross-coupling model reaction. The PdNPs@g-C₃N₄-BLE nanocatalyst was used up to 12th recycles without significant decline in activity as shown in Fig. 9. Furthermore, the 12 times recycled PdNPs@g-C₃N₄-BLE nanocatalyst was characterized by FT-IR (Fig. 1e) and FE-SEM (Fig. 6d) analysis and no noticeable change in the chemical composition or morphology of the PdNPs@g-C₃N₄-BLE nanocatalyst were observed.
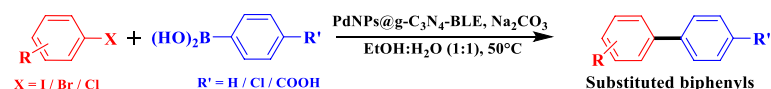
3.3.3 Heterogeneity study of PdNPs@g-C₃N₄-BLE nanocatalyst

To better understand the heterogeneity of the PdNPs@g-C₃N₄-BLE nanocatalyst, a hot filtration test was performed. The model Suzuki–Miyaura cross-coupling reaction was performed under optimized conditions for 1 h. Then the PdNPs@g-C₃N₄-BLE nanocatalyst was separated from the reaction mixture, and the reaction continued under TLC monitoring. We observed no further conversion up to 2 h, and the isolated yield was 50% which was also confirmed by GC–MS analysis (see supporting information). This shows that there is no leaching of palladium from the nanocatalyst into the reaction mass, proving the heterogeneous nature of the PdNPs@g-C₃N₄-BLE nanocatalyst [60].

3.3.4 Comparison of catalysts in Suzuki–Miyaura cross-coupling reaction

In order to understand the significance of the PdNPs@g-C₃N₄-BLE nanocatalyst, we compared the Suzuki–Miyaura cross-coupling reaction of the PdNPs@g-C₃N₄-BLE nanocatalyst between 4-iodoanisole and phenylboronic acid with those for other catalysts reported in literature (Table 4). The results show that the PdNPs@g-C₃N₄-BLE nanocatalyst has superior catalytic activity at moderate temperature in green medium (EtOH:H₂O (1:1)). The PdNPs@g-C₃N₄-BLE nanocatalyst has several key advantages such as short reaction time, mild reaction conditions, use of green solvents, good selectivity, reusability for subsequent reactions, cost-effectiveness, and ease of manufacture.

Table 3 Suzuki–Miyaura cross-coupling reactions between aryl halides with aryl boronic acids by using PdNPs@g-C$_3$N$_4$-BLE nanocatalyst[a]

$$\text{R} \longrightarrow \text{X} + (\text{HO})_2\text{B} \longrightarrow \text{R}' \xrightarrow[\text{EtOH:H}_2\text{O (1:1), 50°C}]{\text{PdNPs@g-C}_3\text{N}_4\text{-BLE, Na}_2\text{CO}_3} \text{Substituted biphenyls}$$

X = I / Br / Cl   R' = H / Cl / COOH

| Entry	Aryl halide	Product	Time (h)	Yield[b] (%)	TON / TOF (h^{-1})
1	H$_3$CO—〇—I	H$_3$CO—〇—〇	2	98	18233 / 9117
2	H$_3$CO—〇—Br	H$_3$CO—〇—〇	3	93	22247 / 7416
3	H$_3$CO—〇—I	H$_3$CO—〇—〇—Cl	2.5	88	16373 / 6549
4	H$_3$CO—〇—Br	H$_3$CO—〇—〇—Cl	3	85	20333 / 6778
5	OCH$_3$ 〇—I	OCH$_3$ 〇—〇	2.5	91	16931 / 6772
6	O$_2$N—〇—I	O$_2$N—〇—〇	2	95	16641 / 8321
7	O$_2$N—〇—Br	O$_2$N—〇—〇	2.25	88	18980 / 8436
8	NC—〇—Br	NC—〇—〇	4	94	22486 / 5622
9	H$_3$C(O)C—〇—Br	H$_3$C(O)C—〇—〇	6	48	10499 / 1750
10	H(O)C—〇—Br	H(O)C—〇—〇	4	72	16941 / 4235
11	O=CH 〇—Br	O=CH 〇—〇	2	38	8941/ 4471
12	H$_3$C—〇—I	H$_3$C—〇—〇	0.75	96	19200 / 25600
13	H$_3$C—〇—Br	H$_3$C—〇—〇	1	95	24216 / 24216
14	〇—I	H—〇—〇	0.16	98	20924 / 130775
15	〇—Br	H—〇—〇	0.25	97	26923 / 107692
16	〇—Cl	H—〇—〇	0.5	85	32889 / 65778
17	H$_3$C—〇—I	H$_3$C—〇—〇—COOH	1	85	17000 / 17000
18	〇—I	H—〇—〇—COOH	1.25	95	20283 / 16226
19	〇—Br	H—〇—〇—COOH	1.25	88	24425 / 19540
20	HO—〇—Br	HO—〇—〇	2.5	90	22667 / 9067
21	O=C(OH)CH$_2$—〇—Br	O=C(OH)CH$_2$—〇—〇	3	93	18843 / 6281

[a]Reaction conditions: aryl halide (1 equiv.), arylboronic acid (1.1 equiv.), PdNPs@g-C$_3$N$_4$-BLE nanocatalyst (2.3 mol% palladium with respect to aryl halide), Na$_2$CO$_3$ (2.2 equiv.), and EtOH:H$_2$O (1:1) (6 mL) in air

[b]Isolated yield after separation by column chromatography; average of two runs

3.4 Catalytic activity of PdNPs@g-C$_3$N$_4$-BLE catalyst in cyanation reaction

Following the Suzuki–Miyaura cross-coupling reaction of aryl halides, we performed cyanation reaction to further explore the catalytic efficiency of the PdNPs@g-C$_3$N$_4$-BLE nanocatalyst. Due to its less hazardous, easily accessibility, and cost-effectiveness, K$_4$[Fe(CN)$_6$].3H$_2$O was chosen as the cyanide source for the cyanation of aryl halides. For the optimization of the reaction conditions, cyanation of 4-bromonitrobenzene was chosen as the model reaction (Scheme 4). Furthermore, the effects of various reaction
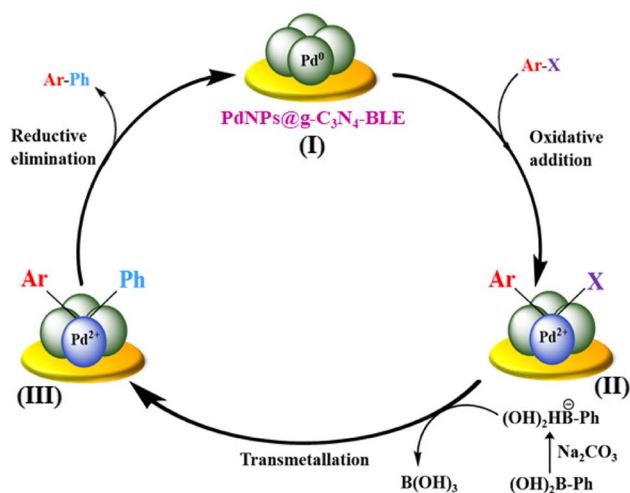
Scheme 3 Proposed mechanism for Suzuki–Miyaura cross-coupling reaction by using PdNPs@g-C$_3$N$_4$-BLE nanocatalyst
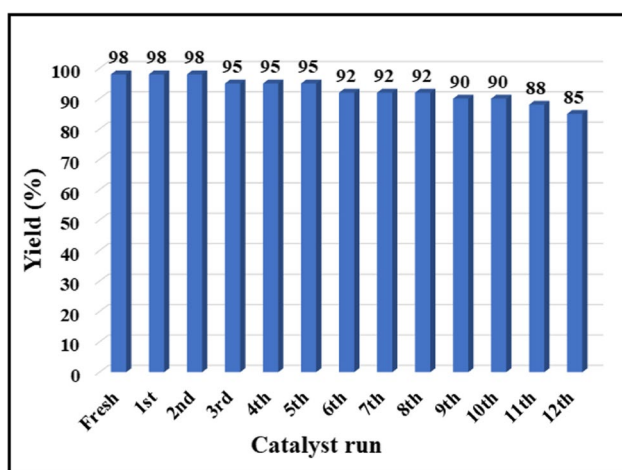

Fig. 9 Recyclability study of the PdNPs@g-C$_3$N$_4$-BLE nanocatalyst in Suzuki–Miyaura cross-coupling of 4-iodoanisole with phenylboronic acid under optimized conditions

parameters such as solvent, base, temperature and catalyst loading were investigated for the model reaction as shown in the Table 5. On analyzing the model reaction using several solvents such as DMF, DMF:H$_2$O (1:1), EtOH and acetonitrile (Table 5, entries 5–8), DMF was discovered to be the best solvent, producing high yield in moderate amount of time (Table 5, entry 5). Likewise, the effect of the PdNPs@g-C$_3$N$_4$-BLE nanocatalyst loading was investigated with 2.3, 2.9 and 3.5 mol% of Pd (Table 5, entries 1–4). The best outcome was obtained with 2.3 mol% of the PdNPs@g-C$_3$N$_4$-BLE nanocatalyst (Table 5, entry 4) at 140 °C. Reaction temperatures ranging from 120 to 140 °C were studied; the product yield was found to increase with the temperature (Table 5, entries 3–5). The bases like

Na$_2$CO$_3$, K$_2$CO$_3$, NaOH, KOH, Cs$_2$CO$_3$, and Et$_3$N were investigated by keeping parameters constant like DMF as solvent and 2.3 mol% of the PdNPs@g-C$_3$N$_4$-BLE nanocatalyst at 140 °C (Table 5, entries 5, 9–13). The best result was given by Na$_2$CO$_3$ and was chosen as the base. From the results obtained the optimized reaction condition for cyanation was attained as DMF as solvent, in presence of Na$_2$CO$_3$ and 2.3 mol% of Pd at 140 °C for 9 h.

3.4.1 Cyanation reactions between aryl halides with K$_4$[Fe(CN)$_6$].3H$_2$O using PdNPs@g-C$_3$N$_4$-BLE nanocatalyst

After establishing the standard reaction conditions for the aryl cyanation reaction, we carried out the substrate scope for various aryl halides (Table 6). The aryl halides, containing both electron withdrawing and electron donating groups such as –NO$_2$, -CN, -CHO, COCH$_3$, and -OCH$_3$, yielded good to outstanding yields. Both aryl iodides and aryl bromides yielded better results in a moderate time (Table 6, entries 1, 2, 7, and 10) with high TONs and TOFs than aryl chlorides which took substantially longer duration of time (Table 6, entries 3 and 11) providing lower yields.

Scheme 5 depicts a plausible mechanism for the catalytic cycle corresponding to the cyanation of aryl halide employing the PdNPs@g-C$_3$N$_4$-BLE nanocatalyst (**I**). The aryl halide undergoes oxidative addition across the Pd NP surface forming the intermediate **II**, followed by ligand exchange from the inner coordination sphere of K$_4$[Fe(CN)$_6$] to the Pd NP-substrate complex (**III**). Finally, aryl nitriles are reductively eliminated from the Pd NP surface, completing the catalytic cycle and regenerating the catalytic site.

3.4.2 Recyclability of the PdNPs@g-C$_3$N$_4$-BLE nanocatalyst in cyanation reaction

The reusability of catalysts is an added advantage to the efficiency of the catalysts. In line with this, the recyclability of the PdNPs@g-C$_3$N$_4$-BLE nanocatalyst was studied for the model reaction between 4-bromonitrobenzene and K$_4$[Fe(CN)$_6$].3H$_2$O. The PdNPs@g-C$_3$N$_4$-BLE nanocatalyst was used up to six runs with slight decrease in catalytic activity as observed in Fig. 10. The FT-IR and FE-SEM analyses of six times recycled PdNPs@g-C$_3$N$_4$-BLE nanocatalyst was recorded (Figs. 1f and 6e). No significant change in the chemical composition and morphology was witnessed from these analyses, which shows that the PdNPs@g-C$_3$N$_4$-BLE nanocatalyst is intact even after 6th recycle.

3.4.3 Comparison of catalysts in cyanation reaction

The activity of the PdNPs@g-C$_3$N$_4$-BLE nanocatalyst for aryl halide cyanation reaction was compared to other

Table 4 Comparison of results for PdNPs@g-C$_3$N$_4$-BLE nanocatalyst with other catalysts for the Suzuki–Miyaura cross-coupling reaction between 4-iodoanisole and phenylboronic acid

Entry	Catalyst	Solvent	Temp. (°C)	Time (h)	Yield (%)	Ref
1	Pd/Fe$_3$O$_4$@charocoal	DMF:H$_2$O (4:1)	100	4	99	[61]
2	Palladacycle adduct catalyst	Dioxane	100	12	93	[62]
3	Catalyst-1	EtOH:H$_2$O (3:1)	70	12	87	[63]
4	NHC-Pd@MNPs	EtOH:H$_2$O (1:1)	70	1	95	[49]
5	γ-Fe2O3-acetamidine-Pd	DMF	100	2	92	[64]
6	Fe$_3$O$_4$/P(GMA-AAMMA)-Schiff base-Pd	DMF:H$_2$O (1:1)	80	1	97	[65]
7	Pd(II)-NiFe2O4	EtOH:H$_2$O (9:1)	80	4	92	[66]
8	GO-2 N-Pd(II)	EtOH	80	4	77	[67]
9	Pd-BC	EtOH	80	1.5	95	[68]
10	GO-NHC-Pd^{2+}	EtOH:H$_2$O (2:1)	60	4	70	[69]
11	**PdNPs@g-C$_3$N$_4$-BLE**	**EtOH:H$_2$O (1:1)**	**50**	**2**	**98**	**Present work**

Bold represents the most effective reaction conditions
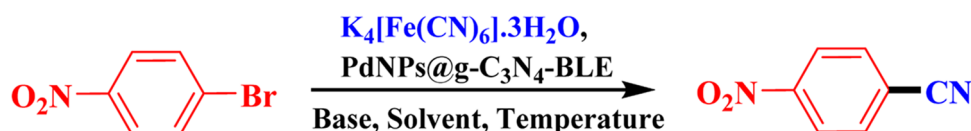
Scheme 4 Cyanation reaction between 4-bromonitrobenzene with K$_4$[Fe(CN)$_6$].3H$_2$O in the presence of the PdNPs@g-C$_3$N$_4$-BLE nanocatalyst

Table 5 Optimization of reaction conditions for cyanation of 4-bromonitrobenzene with K$_4$[Fe(CN)$_6$].3H$_2$O^a

Entry	Base	Solvent	Temp. (°C)	Pd (mol%)	Time (h)	Yield^b (%)
1	Na$_2$CO$_3$	DMF	120	3.5	9	51
2	Na$_2$CO$_3$	DMF	120	2.9	9	45
3	Na$_2$CO$_3$	DMF	120	2.3	8	48
4	Na$_2$CO$_3$	DMF	130	2.3	24	76
5	**Na$_2$CO$_3$**	**DMF**	**140**	**2.3**	**9**	**98**
6	Na$_2$CO$_3$	DMF:H$_2$O (1:1)	140	2.3	16	32
7	Na$_2$CO$_3$	EtOH	140	2.3	16	NR
8	Na$_2$CO$_3$	Acetonitrile	140	2.3	16	48
9	K$_2$CO$_3$	DMF	140	2.3	9	72
10	NaOH	DMF	140	2.3	16	44
11	KOH	DMF	140	2.3	16	35
12	Cs$_2$CO$_3$	DMF	140	2.3	17	45
13	Et$_3$N	DMF	140	2.3	18	32

Bold value indicates the best reaction condition among the sets of reactions performed

^{a}Reaction conditions: 4-bromonitrobenzene (1 equiv.), K$_4$[Fe(CN)$_6$].3H$_2$O (0.17 equiv.), PdNPs@g-C$_3$N$_4$-BLE (2.3 mol% palladium with respect to aryl halide), base (1.5 equiv.), and solvent (5 mL) in air
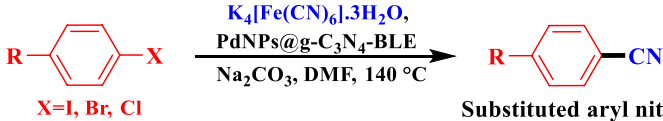
^{b}Isolated yield after separation by column chromatography; average of two runs

known catalytic systems and is tabulated in Table 7. The PdNPs@g-C$_3$N$_4$-BLE nanocatalyst showed the advantages of moderate reaction conditions, low catalyst loading, and shorter reaction time, as well as recyclability and a green synthesis process.

3.5 Antimicrobial activity of g-C$_3$N$_4$ and PdNPs@g-C$_3$N$_4$-BLE nanocatalyst

The antimicrobial activity of the PdNPs@g-C$_3$N$_4$-BLE nanocatalyst and g-C$_3$N$_4$ and their comparison with

Table 6 Cyanation reactions of different aryl halides with $K_4[Fe(CN)_6].3H_2O$ by using PdNPs@g-C$_3$N$_4$-BLE nanocatalyst[a]

$$R-\text{C}_6\text{H}_4-X \xrightarrow[\text{Na}_2\text{CO}_3, \text{DMF, 140 °C}]{K_4[Fe(CN)_6].3H_2O, \text{ PdNPs@g-C}_3\text{N}_4\text{-BLE}} R-\text{C}_6\text{H}_4-\text{CN}$$

X=I, Br, Cl   Substituted aryl nitrile

Entry	Aryl halide	Product	Time (h)	Yield[b] (%)	TON / TOF (h^{-1})
1	⬡—I	⬡—CN	4	94	20070 / 5018
2	⬡—Br	⬡—CN	5	91	25258 / 5052
3	⬡—Cl	⬡—CN	6	68	26311 / 4385
4	O_2N—⬡—Br	O_2N—⬡—CN	9	98	21137 / 2349
5	O_2N—⬡—I	O_2N—⬡—CN	8	95	16641 / 2080
6	H_3CO—⬡—I	H_3CO—⬡—CN	10	91	16931 / 1693
7	H_3CO—⬡—Br	H_3CO—⬡—CN	11	84	19582 / 1780
8	NC—⬡—Br	NC—⬡—CN	10	93	22247 / 2225
9	OHC—⬡—Br	OHC—⬡—CN	13	94	22118 / 1701
10	H_3CCO—⬡—Br	H_3CCO—⬡—CN	11	85	18593 / 1690
11	H_3CCO—⬡—Cl	H_3CCO—⬡—CN	11	42	11841 / 1076

[a]Reaction conditions: 4-bromonitrobenzene (1 equiv.), $K_4[Fe(CN)_6].3H_2O$ (0.17 equiv.), PdNPs@g-C$_3$N$_4$-BLE (2.3 mol% palladium with respect to aryl halide), Na$_2$CO$_3$ (1.5 equiv.), and DMF (5 mL) in air

[b]Isolated yield after separation by column chromatography; average of two runs
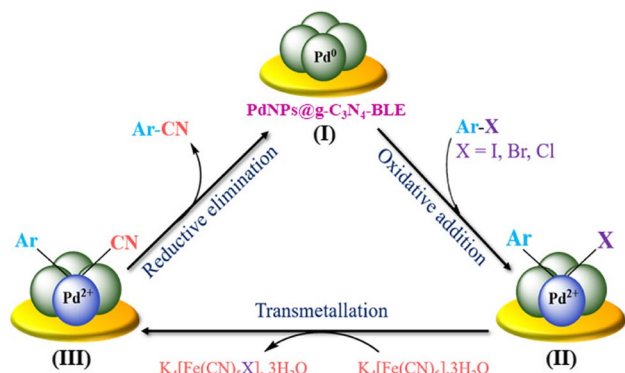
Scheme 5 Proposed mechanism for PdNPs@g-C$_3$N$_4$-BLE catalyzed cyanation reaction

Fig. 10 Recyclability of the PdNPs@g-C$_3$N$_4$-BLE nanocatalyst in cyanation reaction between 4-bromonitrobenzene with $K_4[Fe(CN)_6].3H_2O$ under optimized conditions

standard streptomycin towards pathogenic strain of gram-negative bacteria *E. coli* and gram-positive bacteria *B. subtilis* are shown in Figs. 11 and 12 respectively. Here, the solvent medium (ethylene glycol:HCl (9:1)) used to
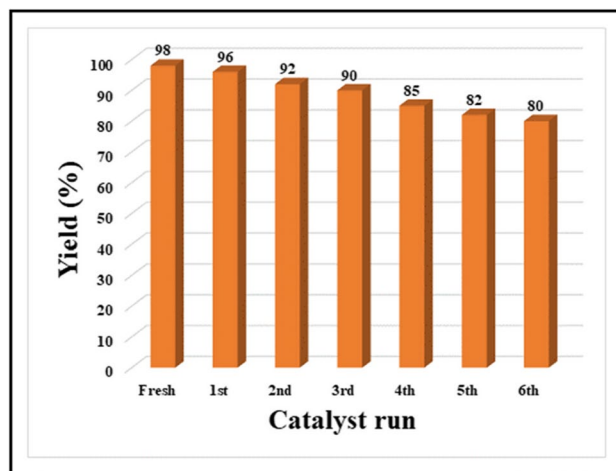
Table 7 Comparison of results for PdNPs@g-C$_3$N$_4$-BLE nanocatalyst with those for other catalysts in cyanation reaction of 4-bromonitrobenzene with K$_4$[Fe(CN)$_6$].3H$_2$O

Entry	Catalyst	Solvent	Temp. (°C)	Time (h)	Yield (%)	Ref
1	Pd@CC$_1^r$/Pd@CC$_2^r$	DMF	140	15	99	[70]
2	Pd(OAc)$_2$	POCl$_3$	140	48	81	[39]
3	Pd(ligand)	DMAc	140	16	82	[71]
4	Pd catalyst	Toluene	160	16	91	[72]
5	Pd$_2$(dba)$_3$	DMA	150	4	88	[73]
6	**PdNPs@g-C$_3$N$_4$-BLE**	**DMF**	**140**	**9**	**98**	**Present work**

Bold represents the most effective reaction conditions

Fig. 11 The ZOI formed by (**a**) PdNPs@g-C$_3$N$_4$-BLE nano-catalyst and (**b**) g-C$_3$N$_4$ against human bacterial pathogen *E. coli*. **1** PdNPs@g-C$_3$N$_4$-BLE nanocatalyst/g-C$_3$N$_4$, **2** distilled water, **3** standard streptomycin, and **4** ethylene glycol:HCl (9:1)
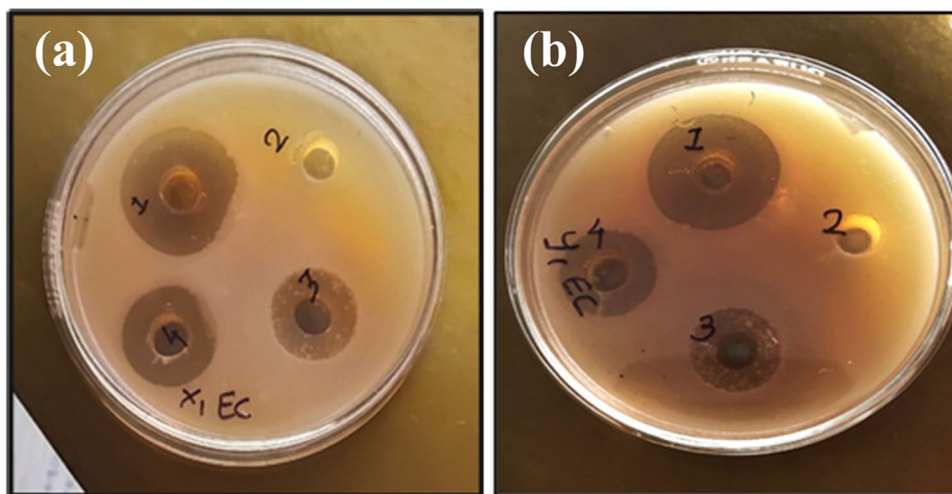
Fig. 12 (**a**) The ZOI formed by (**a**) PdNPs@g-C$_3$N$_4$-BLE nano-catalyst and (**b**) g-C$_3$N$_4$ against human bacterial pathogen *B. subtilis*. **1** PdNPs@g-C$_3$N$_4$-BLE nanocatalyst/g-C$_3$N$_4$, **2** distilled water, **3** standard streptomycin, and **4** ethylene glycol:HCl (9:1)
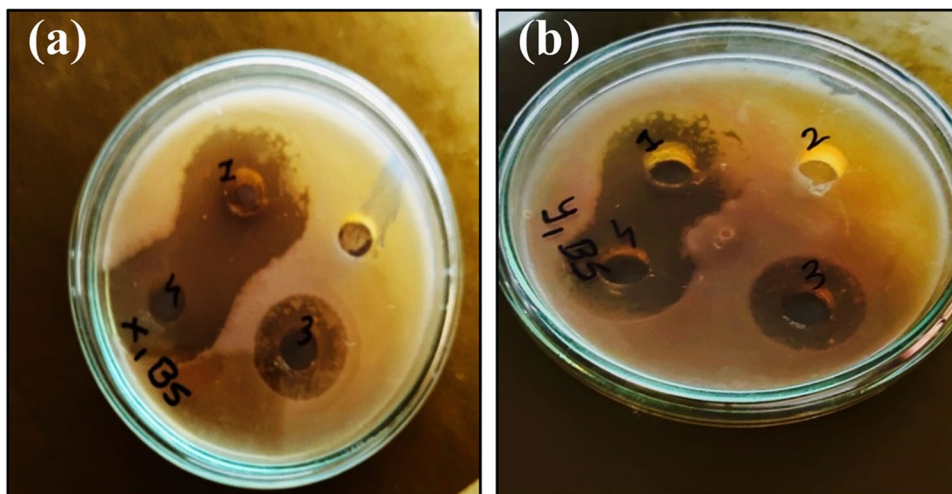
dissolve both the g-C$_3$N$_4$ and PdNPs@g-C$_3$N$_4$-BLE nano-catalyst showed some antimicrobial property. Hence, zone of inhibition (ZOI) of the solvent was subtracted from the ZOI of g-C$_3$N$_4$ and PdNPs@g-C$_3$N$_4$-BLE nanocatalyst to get the actual zone of inhibition of the desired compounds. The results revealed the antimicrobial activity of PdNPs@g-C$_3$N$_4$-BLE to be superior to g-C$_3$N$_4$ with a ZOI of 8 and 10 mm against *E. coli* and *B. subtilis* respectively.

The results are tabulated in Table 8. The biogenically synthesized PdNPs@g-C$_3$N$_4$-BLE nanocatalyst has shown anti-microbial activity due to its high surface-volume ratio compared to the chemically synthesized Pd NPs. The interaction of Pd NPs with microorganism may lead to the rupture of the bacterial cell wall which ultimately disturbs the functioning of cells resulting in the death of the microorganism [74].

Table 8 Antimicrobial properties of g-C_3N_4 and PdNPs@g-C_3N_4-BLE

Sl. No	Name of the compound	Mean ZOI observed in case of *E. coli*	Mean ZOI observed in case of *B. subtilis*
1	g-C_3N_4	7 mm	6 mm
2	PdNPs@g-C_3N_4-BLE	8 mm	10 mm
3	Streptomycin	15 mm	9 mm
4	Water	No ZOI	No ZOI

4 Conclusions

In summary, we reported the in situ biogenic synthesis of palladium nanoparticles embedded on banana leaves extract-modified graphitic carbon nitride (PdNPs@g-C_3N_4-BLE) as a competent nanocatalyst by green and sustainable protocol. The characterization of the PdNPs@g-C_3N_4-BLE nanocatalyst by various analytical techniques confirmed its structure, morphology, composition, and stability. The PdNPs@g-C_3N_4-BLE nanocatalyst has essential key features like eco-friendly, simple design, common reagents, high activity, and selectivity towards Suzuki–Miyaura cross-coupling and cyanation of aryl halide reactions. Moreover, the PdNPs@g-C_3N_4-BLE nanocatalyst showed broad range of functional groups tolerance, yielding substituted biphenyls with 72–98% (21 examples) in Suzuki–Miyaura cross-coupling and substituted aryl nitriles with 68–98% (11 examples) in cyanation reaction. In both the reactions, the PdNPs@g-C_3N_4-BLE nanocatalyst was reused successfully up to 12th and 6th recycles for Suzuki-Miyuara cross-coupling and cyanation reactions respectively, without substantial decline of catalytic activity. Besides, we also synthesized the NSAID Felbinac in greener reaction conditions utilizing the PdNPs@g-C_3N_4-BLE nanocatalyst. To broaden the scope of applicability of the PdNPs@g-C_3N_4-BLE nanocatalyst in the field of medicinal chemistry, its antimicrobial activity was investigated, where it showed reasonable antimicrobial activity against gram-positive bacteria *E. coli* and gram-negative bacteria *B. subtilis*. Herein we believe that the newly developed methodology will add great utility academically and industrially, and can be surveyed for other possible applications.

Availability of data and materials Not applicable.

Declarations

Ethical approval and consent to participate Not applicable.

Competing interests The authors declare no competing interests.

References

1. Nasrollahzadeh M, Sajadi SM, Sajjadi M, Issaabadi (2019) An introduction to nanotechnology. Interface Sci Technol 28:1–27
2. Burda C, Chen X, Narayanan R, El-sayed MA (2005) Chemistry and properties of nanocrystals of different shapes. Chem Rev 105:1025–1102
3. Salem SS, Fouda A (2020) Green synthesis of metallic nanoparticles and their prospective biotechnological applications: an overview. Biol Trace Elem Res 199:344–370
4. Chen Z, Vorobyeva E, Mitchell S, Fako E, Ortuño MA, López N, Collins SM, Midgley PA, Richard S, Vilé G, Pérez-Ramírez J (2018) A heterogeneous single-atom palladium catalyst surpassing homogeneous systems for Suzuki coupling. Nat Nanotechnol 13:702–707
5. Devi M, Barbhuiya MH, Das B, Bhuyan B, Dhar SS (2020) Modified mesoporous graphitic carbon nitride: a novel high-performance heterogeneous base catalyst for transesterification reaction. Sustain Energy Fuels 4:3537–3545
6. Kalay E (2022) Investigation of the activity of palladium nanoparticles supported on mesoporous graphitic carbon nitride in Heck and Suzuki cross-coupling reactions. Synth Commun 52:1290–1305
7. Yang P, Ma R, Bian F (2016) Palladium supported on metformin-functionalized magnetic polymer nanocomposites: a highly efficient and reusable catalyst for the Suzuki-Miyaura coupling reaction. ChemCatChem 8:3746–3754
8. Aksoy M, Kilic H, Nişancı B, Metin Ö (2021) Recent advances in the development of palladium nanocatalysts for sustainable organic transformations. Inorg Chem Front 8:499–545
9. Mallikarjuna K, Reddy LV, Al-Rasheed S, Mohammed A, Gedi S, Kim WK (2021) Green synthesis of reduced graphene oxide-supported palladium nanoparticles by *Coleus amboinicus* and its enhanced catalytic efficiency and antibacterial activity. Curr Comput-Aided Drug Des 11(2):134
10. Kumar R, Sharma P, Bamal A, Negi S, Chaudhary S (2017) A safe, efficient and environment friendly biosynthesis of silver nanoparticles using Leucaena leucocephala seed extract and its antioxidant, antimicrobial, antifungal activities and potential in sensing. Green Process Synth 6(5):449–459

11. Adil SF, Assal ME, Khan M, Al-Warthana A, Siddiqui MRH, Liz-Marzan LM (2015) Biogenic synthesis of metallic nanoparticles and prospects toward green chemistry. Dalton Trans 44(21):9709–9717

12. Bognár S, Putnik P, Merkulov DŠ (2022) Sustainable green nanotechnologies for innovative purifications of water: synthesis of the nanoparticles from renewable sources. Nanomaterials 12:263

13. Onyema C, Ogbuagu AS (2016) Phytochemical and antimicrobial analysis of banana pseudo stem (Musa acuminata). Br J Pharm Res 10(1):1–9

14. Dwivedi KD, Borah B, Chowhan LR (2020) Ligand free one-pot synthesis of pyrano [2, 3-c] pyrazoles in water extract of banana peel (WEB): a green chemistry approach. Front Chem 7:944

15. Kibria AA, Kamrunnessa RM, Kar A (2019) Extraction and evaluation of phytochemicals from banana peels (Musa sapientum) and banana plants (Musa paradisiaca). MJHR 2:22–26

16. Chng LL, Erathodiyil N, Ying JY (2013) Nanostructured catalysts for organic transformations. Acc Chem Res 46(8):1825–1837

17. Ghafuri H, Gorab MG, Dogari H (2022) Tandem oxidative amidation of benzylic alcohols by copper(II) supported on metformin-graphitic carbon nitride nanosheets as an efficient catalyst. Sci Rep 12:4221

18. Mao C, Yin K, Yang C, Dong G, Tian G, Zhang Y, Zhou Y (2022) Fe-based MOFs@Pd@COFs with spatial confinement effect and electron transfer synergy of highly dispersed Pd nanoparticles for Suzuki-Miyaura coupling reaction. J Colloid Interface Sci 608:809–819

19. Kang HJ, Lee TG, Bari GAKMR, Seo HW, Park JW, Hwang HJ, An BH, Suzuki N, Fujishima A, Kim JH, Shon HK, Jun YS (2021) Sulfuric acid treated g-CN as a precursor to generate high-efficient g-CN for hydrogen evolution from water under visible light irradiation. Catalysts 11(1):37

20. Shcherban ND, Mäki-Arvela P, Aho A, Sergiienko SA, Yaremov PS, Eränenb K, Murzin DY (2018) Melamine-derived graphitic carbon nitride as a new effective metal-free catalyst for Knoevenagel condensation of benzaldehyde with ethylcyanoacetate. Catal Sci Technol 8:2928–2937

21. Bayrak C, Menzek A, Sevim M (2020) Monodisperse NiPd alloy nanoparticles decorated on mesoporous graphitic carbon nitride as catalyst for the highly efficient chemoselective reduction of α, β-unsaturated ketone compounds. New J Chem 44:13606–13612

22. Eswaran M, Dhanusuraman R, Tsai P, Ponnusamy VK (2019) One-step preparation of graphitic carbon nitride/polyaniline/palladium nanoparticles based nanohybrid composite modified electrode for efficient methanol electro-oxidation. Fuel 251:91–97

23. Nasri A, Jaleh B, Nezafat Z, Nasrollahzadeh M, Azizian S, Jang HW, Shokouhimehr M (2021) Fabrication of g-C$_3$N$_4$/Au nanocomposite using laser ablation and its application as an effective catalyst in the reduction of organic pollutants in water. Ceram Int 47(3):3565–3572

24. Lima CFRAC, Rodrigues ASMC, Silva VLM, Silva AMS, Santos LMNBF (2014) Role of the base and control of selectivity in the Suzuki – Miyaura cross-coupling reaction. ChemCatChem 61291–302

25. Lennox AJJ, Lloyd-jones GC (2014) Selection of boron reagents for Suzuki – Miyaura coupling. Chem Soc Rev 43:412–443

26. Mohazzab BF, Jaleh B, Issaabadi Z, Nasrollahzadeh M, Varma RS (2019) Stainless steel mesh-GO/Pd NPs: catalytic applications of Suzuki-Miyaura and Stille coupling reactions in eco-friendly media. Green Chem 21:3319–3327

27. Miyaura N, Yanagi T, Suzuki A (1981) The palladium-catalyzed cross coupling reaction of phenylboronic acid with haloarenes in the presence of bases. Synth Commun 11(7):513–519

28. Li G, Lei P, Szostak M, Casals-cruañas E, Poater A, Cavallo L, Nolan SP (2018) Mechanistic study of Suzuki-Miyaura cross-coupling reactions of amides mediated by [Pd(NHC)(allyl) Cl] precatalysts. ChemCatChem 10(14):3096–3106

29. Baran T, Mentes A (2016) Microwave assisted synthesis of biaryls by C-C coupling reactions with a new chitosan supported Pd(II) catalyst. J Mol Struct 1122:111–116

30. Baran T (2019) Highly recoverable, reusable, cost-effective, and Schiff base finctionalized pectin supported Pd(II) catalyst for microwave-accelerated Suzuki cross-coupling reactions. Int J Biol Macromol 127:232–239

31. Baran T, Nasrollahzadeh M (2020) Cyanation of aryl halides and Suzuki-Miyaura coupling reaction using palladium nanoparticles anchored on developed biodegradable microbeads. Int J Biol Macromol 148:565–573

32. Melike Ç, Baran T, Nasrollahzadeh M (2021) Facile preparation of nanostructured Pd-Sch-δ-FeOOH particles: a highly effective and easily retrievable catalyst for aryl halide cyanation and p-nitrophenol reduction. J Phys Chem Solids 152:109968

33. Baran T, Sargın İ, Kaya M, Mulerčikas P, Kazlauskaitė S, Menteş A (2018) Production of magnetically recoverable, thermally stable, bio-based catalyst: remarkable turnover frequency and reusability in Suzuki coupling reaction. Chem Eng J 331:102–113

34. Veisi H, Tamoradi T, Karmakar B, Mohammadi P, Hemmati S (2019) In situ biogenic synthesis of Pd nanoparticles over reduced graphene oxide by using a plant extract (Thymbra spicata) and its catalytic evaluation towards cyanation of aryl halides. Mater Sci Eng C 104:109919

35. Yu H, Richey RN, Miller WD, Xu J, May SA (2011) Development of Pd/C-catalyzed cyanation of aryl halides. J Org Chem 76(2):665–668

36. Ushkov AV, Grushin VV (2011) Rational catalysis design on the basis of mechanistic understanding: highly efficient Pd-catalyzed cyanation of aryl bromides with NaCN in recyclable solvents. J Am Chem Soc 133:10999–11005

37. Anbarasan P, Schareina T, Beller M (2011) Recent developments and perspectives in palladium-catalyzed cyanation of aryl halides: synthesis of benzonitriles. Chem Soc Rev 40:5049–5067

38. Chang S, Kim J, Kim HJ, Chang S (2012) Synthesis of aromatic nitriles using nonmetallic cyano-group sources. Angew Chem Int Ed Engl 51(48):11948–11959

39. Sawant DN, Wagh YS, Tambade PJ, Bhatte KD, Bhanage BM (2011) Cyanides-free cyanation of aryl halides using formamide. Adv Synth Catal 353(5):781–787

40. Kandathil V, Dateer RB, Sasidhar BS, Patil SA, Patil SA (2018) Green synthesis of palladium nanoparticles: applications in aryl halide cyanation and Hiyama cross-coupling reaction under ligand free conditions. Catal Lett 148:1562–1578 (and references cited therein)

41. Veisi H (2019) Efficient cyanation of aryl halides with K4[Fe(CN)6] catalyzed by encapsulated palladium nanoparticles in biguanidine–chitosan matrix as core–shell recyclable heterogeneous nanocatalyst. Polyhedron 159:212–216

42. Lemire JA, Harrison JJ, Turner RJ (2013) Antimicrobial activity of metals: mechanisms, molecular targets and applications. Nat Rev Microbiol 11:371–384

43. Bhatt P, Pandey SC, Joshi S, Chaudhary P, Pathak VM, Huang Y, Wu X, Zhou Z, Chen S (2022) Nanobioremediation: a sustainable approach for the removal of toxic pollutants from the environment. J Hazard Mater 427:128033

44. Sajjadi M, Nasrollahzadeh M, Tahsili MR (2019) Catalytic and antimicrobial activities of magnetic nanoparticles supported N -heterocyclic palladium (II) complex : a magnetically recyclable catalyst for the treatment of environmental contaminants in aqueous media. Sep Purif Technol 227:115716–115719

45. Vijilvani C, Bindhu MR, Frincy FC, AlSalhi MS, Sabitha S, Saravanakumar K, Devanesan S, Umadevi M, Aljaafreh MJ, Aljaafreh MJ, Atif M (2019) Antimicrobial and catalytic

activities of biosynthesized gold, silver and palladium nanoparticles from Solanum nigrum leaves. J Photochem Photobiol B: Biol 202:111713

46. Wang L, Hu C, Shao L (2017) The antimicrobial activity of nanoparticles : present situation and prospects for the future. Int J Nanomed 12:1227–1249

47. Kempasiddaiah M, Kandathil V, Dateer RB, Sasidhar BS, Patil SA, Patil SA (2020) Immobilizing biogenically synthesized palladium nanoparticles on cellulose support as a green and sustainable dip catalyst for cross-coupling reaction. Cellulose 27:23335–23357

48. Antony AM, Kandathil V, Kempasiddaiah M, Sasidhar BS, Patil SA, Patil SA (2020) Hexagonal boron nitride supported N-heterocyclic carbene-palladium(II): a new, efficient and recyclable heterogeneous catalyst for Suzuki-Miyaura cross-coupling reaction. Catal Lett 151:1293–1308

49. Vishal K, Fahlman BD, Sasidhar BS, Patil SA, Patil SA (2017) Magnetic nanoparticle-supported N-heterocyclic carbene-palladium(II): a convenient, efficient and recyclable catalyst for Suzuki-Miyaura cross-coupling reactions. Catal Lett 147(4):900–918

50. Kempasiddaiah M, Sree Raj KA, Kandathil V, Dateer RB, Sasidhar BS, Yelamaggad CV, Rout CS, Patil SA (2021) Waste biomass-derived carbon-supported palladium-based catalyst for cross-coupling reactions and energy storage applications. Appl Surf Sci 570:151156

51. Wang Y, Zhao S, Zhang Y, Fang J, Chen W, Yuan S, Zhou Y (2018) Facile synthesis of self-assembled g-C3N4 with abundant nitrogen defects for photocatalytic hydrogen evolution. ACS Sustain Chem Eng 6:10200–10210

52. Xu J, Chen Y, Hong Y, Zheng H, Ma D, Xue B, Li Y (2018) Direct catalytic hydroxylation of benzene to phenol catalyzed by vanadia supported on exfoliated graphitic carbon nitride. Appl Catal A: Gen 549:31–39

53. Ma J, Liang C, Li H, Xu H, Hua Y, Wang C (2021) A novel composite material based on hydroxylated g-C3N4 and oxygen-vacant TiO2 for improvement of photocatalytic performance. Appl Surf Sci 546:149085

54. Ushie OA, Onen AI, Ugbogu OC, Olumide VB (2016) Phytochemical screening and antimicrobial activities of leaf extracts of Swietenia macrophylla. Chemsearch J 7(2):64–69

55. Sheikh MV, Devadiga N, Hate M (2016) Biosynthesis and kinetic studies of silver nanoparticles from semecarpus anacardium linn.f and their application. World J Pharm Pharm Sci 4:1732–1739

56. Li X, Zhang J, Shen L, Ma Y, Lei W, Cui Q, Zou G (2009) Preparation and characterization of graphitic carbon nitride through pyrolysis of melamine. Appl Phys A: Mater Sci Process 94:387–392

57. Xu J, Gan YL, Pei JJ, Xue B (2020) Metal-free catalytic conversion of CO_2 into cyclic carbonate by hydroxyl-functionalized graphitic carbon nitride materials. Mol Catal 491:110979

58. Sherwood J, Clark JH, Fairlamb IJS, Slattery JM (2019) Solvent effects in palladium catalysed cross-coupling reactions. Green Chem 21:2164–2213

59. Edwards GA, Trafford MA, Hamilton AE, Buxton AM, Bardeaux MC, Chalker JM (2014) Melamine and melamine-formaldehyde polymers as ligands for palladium and application to Suzuki-Miyaura cross-coupling reactions in sustainable solvents. J Org Chem 79(5):2094–2104

60. Çalıskan M, Baran T (2022) Immobilized palladium nanoparticles on Schiff base functionalized ZnAl layered double hydroxide: a highly stable and retrievable heterogeneous nanocatalyst towards aryl halide cyanations. Appl Clay Sci 219:106433

61. Woo H, Lee K, Park JC, Park KH (2014) Facile synthesis of Pd/Fe3O4/charcoal bifunctional catalysts with high metal loading for high product yields in Suzuki-Miyaura coupling reactions. New J Chem 38:5626–5632

62. Bai SZ, Xu C, Li HM, Wang ZQ, Fu WJ (2012) Synthesis and characterization of triphenylphosphine adducts of ferrocene-based palladacycles and their performance in the Suzuki and Sonogashira reactions with bromo- and chloroarenes. Molecules 17:5532–5543

63. Wang Z, Yu Y, Zhang YX, Li SZ, Qian H, Lin ZY (2015) A magnetically separable palladium catalyst containing a bulky N-heterocyclic carbene ligand for the Suzuki-Miyaura reaction. Green Chem 17(1):413–420

64. Sobhani S, Ghasemzadeh MS, Honarmand M, Zarifi F (2014) Acetamidine-palladium complex immobilized on γ-Fe2O3 nanoparticles: a novel magnetically separable catalyst for Heck and Suzuki coupling reactions. RSC Adv 4:44166–44175

65. Yuan D, Chen L, Yuan L, Liao S, Yang M, Zhang Q (2016) Superparamagnetic polymer composite microspheres supported Schiff base palladium complex: an efficient and reusable catalyst for the Suzuki coupling reactions. Chem Eng Sci 287:241–251

66. Singh AS, Shelkar RS, Nagarkar JM (2015) Palladium(II) on functionalized NiFe2O4: an efficient and recyclable phosphine-free heterogeneous catalyst for Suzuki coupling reaction. Catal Lett 145:723–730

67. Bai C, Zhao Q, Li Y, Zhang G, Zhang F, Fan X (2014) Palladium complex immobilized on graphene oxide as an efficient and recyclable catalyst for Suzuki coupling reaction. Catal Lett 144:1617–1623

68. Xiang Z, Chen Y, Liu Q, Lu F (2018) A highly recyclable dip-catalyst produced from palladium nanoparticle-embedded bacterial cellulose and plant fibers. Green Chem 20:1085–1094

69. Shang N, Feng C, Zhang H, Gao S, Tang R, Wang C, Wang Z (2013) Suzuki-Miyaura reaction catalyzed by graphene oxide supported palladium nanoparticles. Chem Commun 40:111–115

70. Mondal B, Acharyya K, Howlader P, Mukherjee PS (2016) Molecular cage impregnated palladium nanoparticles: efficient, additive-free heterogeneous catalysts for cyanation of aryl halides. J Am Chem Soc 138:1709–1716

71. Schareina T, Jackstell R, Schulz T, Zapf A, Cotté A, Gotta M, Beller M (2009) Increasing the scope of palladium-catalyzed cyanations of aryl chlorides. Adv Synth Catal 351:643–648

72. Sundermeier M, Zapf A, Beller M, Sans J (2001) A new palladium catalyst system for the cyanation of aryl chlorides. Tetrahedron Lett 42:6707–6710

73. Jin F, Confalone PN (2000) Palladium-catalyzed cyanation reactions of aryl chlorides. Tetrahedron Lett 41:3271–3273

74. Singh R, Smitha MS, Singh SP (2014) The role of nanotechnology in combating multi-drug resistant bacteria. J Nanosci Nanotechnol 14:4745–4756